scientific reports

Check for updates

OPEN

Green synthesis of *Brassica carinata* microgreen silver nanoparticles, characterization, safety assessment, and antimicrobial activities

Dogfounianalo Somda[1,2]✉, Joel L. Bargul[3], John M. Wesonga[4] & Sabina Wangui Wachira[5]

Nanotechnology has been a central focus of scientific investigation over the past decades owing to its versatile applications. The synthesis of silver nanoparticles (AgNPs) through plant secondary metabolites is a cost-effective and eco-friendly approach. The present study employed *Brassica carinata* microgreen extracts (BCME) to promote the reduction of silver nitrate ($AgNO_3$) salt into *Brassica carinata* microgreen silver nanoparticles (*BCM*-AgNPs). The physicochemical properties of the biosynthesized AgNPs were characterized through both spectroscopy and microscopy techniques. Furthermore, the antimicrobial property of the biosynthesized AgNPs was assessed against six selected pathogenic microorganisms, and finally, their safety was evaluated on a normal Vero cell line through an MTT cytotoxicity assay. The UV-visible spectrum revealed that *BCM*-AgNPs exhibited an absorption peak at 420 nm. The potential functional groups involved in the biosynthesis of AgNPs were identified by Fourier transform infrared (FTIR) analysis. Scanning electron microscopy (SEM) revealed a spherical nature of the biosynthesized AgNPs. Transmission electron microscopy (TEM) analysis revealed the crystallinity of the AgNPs, averaging 34.68 nm in size. X-ray diffraction (XRD) investigation further confirmed the crystalline structure of the AgNPs. The zeta potential exhibited a significant value of -22.5 ± 1.16 mV. Regarding the antimicrobial potential, *BCM*-AgNPs exhibited promising antimicrobial activity against the tested pathogens, with a minimum inhibitory concentration (MIC) of 62.5 µg/mL observed in *Pseudomonas aeruginosa*. Further cytotoxicity assessment of *BCM*-AgNPs conducted on Vero cells demonstrated their safety. This study presents a novel approach to synthesizing AgNPs using a nutraceutical microgreen, offering a biocompatible and promising alternative for combating multi-drug resistance.

Keywords Silver nanoparticles, Green synthesis, *Brassica carinata* microgreen, Antimicrobial property, Safety assessment

Nanoscience focuses on investigating and managing materials at the nanometer scale, where their properties differ from those of bulk materials due to quantum effects and a significant surface area-to-volume ratio[1–3]. Nanotechnology, the application of nanoscience, has experienced rapid growth worldwide and has applications in biomedicine, agriculture, and environmental remediation[1,2]. The combination of biotechnology and nanotechnology has given rise to nanobiotechnology, which enables eco-friendly product manufacturing and advances in biosynthetic technology for the synthesis of nanomaterials. Nanoparticles are atoms organized within a size range of 1 to 100 nanometers[4].

[1]Department of Molecular Biology and Biotechnology, Pan African University Institute for Basic Sciences, Technology, and Innovation (PAUSTI), P.O. Box 62000-00200, Nairobi, Kenya. [2]Laboratory of Molecular Biology and Genetics (LABIOGENE), Joseph Ki-Zerbo University, P.O. Box 7021, Ouagadougou 03, Burkina Faso. [3]Department of Biochemistry, Jomo Kenyatta University of Agriculture and Technology (JKUAT), P.O. Box 62000-00200, Nairobi, Kenya. [4]Department of Horticulture and Food Security, Jomo Kenyatta University of Agriculture and Technology (JKUAT), P.O. Box 62000-00200, Nairobi, Kenya. [5]Centre for Traditional Medicine and Drug Research, Kenya Medical Research Institute (KEMRI), P.O. Box 54840-00200, Nairobi, Kenya. ✉email: metuorssomda@gmail.com

Metallic nanoparticles are receiving significant attention in the medical field due to their distinctive electrical, chemical, optical, and catalytic properties. These properties make them highly valuable as potential agents for transportation, diagnosis, therapy, and drug delivery[5–7]. Metallic nanoparticles consist of various types, namely gold, copper, zinc, and AgNPs, among others. AgNPs have gained prominence among metallic nanoparticles because they are versatile and possess excellent physical, chemical, and biological properties mainly attributed to their size, shape, composition, crystallinity, and structure[4]. Moreover, AgNPs are known to have high antimicrobial, antiviral, and anticancer activity among the most commonly used nanoparticles. Several approaches exist for synthesizing nanoparticles, including chemical, physical, and biological methods[8,9]. However, employing plant extracts to synthesize AgNPs offers numerous benefits over other methods[10,11]. The use of plant extracts eliminates the need for dangerous reducing and capping chemicals[11,12], excessive heat, radiation, and expensive microbial growth media and strains in the process of nanoparticle synthesis[13,14]. Furthermore, plant-mediated synthesis is a rapid, reliable, safe, cost-effective, eco-friendly, and straightforward method[3]. On the other hand, green synthesis of nanoparticles through plant extract leads to nanoparticles that are biocompatible and biodegradable, ensuring their safety in numerous applications, especially bioapplication[14,15]. The synthesis of AgNPs from plant extracts has gained significant attention due to the aforementioned benefits and promising applications. Scientists have explored the application of photosynthesized AgNPs in biomedical diagnostics, namely as antibacterial, anti-inflammatory, and anticancer substances[3,16]. The biomolecules found in plant extracts, such as amino acids, proteins, enzymes, and vitamins, act as reducing, stabilizing, and capping agents in the nanoparticle synthesis process by facilitating the reduction of silver ions (Ag^{+}) to silver atoms (Ag^{0})[17,18]. The shape and size of AgNPs significantly influence their electronic and optical properties, which in turn affects their bioactivity[4,19–21]. AgNPs with identical surface areas but different shapes exhibit varying levels of bactericidal activity[22,23]. This difference is due to the variations in effective surface areas and active facets of the AgNPs. Therefore, it is essential to control these parameters as well as the surrounding medium during the synthesis of AgNPs[24].

The global incidence of infectious diseases has significantly increased due to the widespread and improper utilization of drugs, resulting in the emergence of antibiotic-resistant microorganisms, also referred to as multi-resistant pathogens[25,26]. These multi-resistant pathogens are responsible for the resurgence of a myriad of health issues along with their associated economic damages. In 2022, approximately five million deaths were associated with drug-resistant infections. This figure is expected to rise to ten million per year by 2050[27].

There is a crucial need to develop new antibacterial agents in order to address antibiotic resistance and effectively manage diseases. AgNPs play a significant role in therapeutic applications as remarkable anticancer, antidiabetic, antioxidant, and antimicrobial agents[3,28–30]. Biosynthesized AgNPs have demonstrated remarkable antimicrobial properties attributed to the phytoconstituents on their surface from green synthesis[31]. These AgNPs can damage bacterial cell membranes, making them excellent agents against antibiotic-resistant bacteria and a cornerstone in the fight against multidrug-resistant pathogens[29]. Plants such as *Azadirachta indica*, *Brassica oleracea*, and *Citrullus colocynthis* have been successfully employed to biosynthesize AgNPs[32,33]. In addition, AgNPs synthesized from extracts of *Datura stramonium*, *Ocimum sanctum*, and *Pyrostegia venusta* leaves have shown a broad spectrum of antimicrobial activity[34].

Microgreens are one of the trending foods used as nutraceuticals. These are young, edible plants harvested after the first true leaves emerge, typically within 7 to 21 days of seeding[35,36]. Microgreens are becoming more popular due to their growing prominence as functional foods with both medicinal and nutritional benefits (nutraceuticals)[37,38]. *Brassicaceae*, *Asteraceae*, *Apiaceae*, *Cucurbitaceae*, *Fabaceae*, and *Lamiaceae* are the leading families that contribute to microgreens[35].

Brassica carinata (commonly referred to as Ethiopian kale) belongs to the African Indigenous Vegetables (ALVs), a group of plants widely cultivated and eaten in eastern and southern Africa[36,39]. This plant, belonging to the *Brassicaceae* family, along with other species, has attracted significant interest as nutraceuticals and microgreens[40]. Scientific interest in these plants stems from their copious amounts of phytochemical compounds, making them valuable for both nutrition and medicine[41]. Prior studies on the mature plant[36,42] as well as microgreens[4] have revealed its potent antioxidant, antibacterial, anti-diabetic, and anticancer properties. Additionally, the leaves and seeds of *Brassica carinata* are rich in nutrients, with high concentrations of glucosinolates, which confer significant therapeutic properties[36]. Economically, *Brassica carinata* serves as a nutritious food source, oilseed crop, and potential biofuel, contributing to sustainable agriculture and enhancing food security in various regions[39].

The efficacy of many medicinal plant species relies on the intake of their active compounds into the body. Nonetheless, when administered as raw extracts, the bioavailability of these active compounds in plant-based medicinal products is notably diminished[43–45]. This challenge can be solved by combining herbal therapy with nanotechnologies because nanosystems can effectively transport bioactive compounds at adequate concentrations over the treatment period, guiding them to specific sites of action, thereby enhancing the potency of the compounds[46,47]. The present study aimed to synthesize and characterize *BCM*-AgNPs, to study their potential bioapplications and safety.

Materials and methods

Growth and preparation of microgreens

Microgreens were grown in a locally fabricated growth chamber at Jomo Kenyatta University of Agriculture and Technology (JKUAT), Nairobi, Kenya (1.0912° S, 37.0117° E). *Brassica carinata* seeds were procured from the local market in Ruiru, Kenya. Authentication of the species (microgreens) was done by comparison to a reference specimen, Ref: JMW/JKUAT/BOT/H001, archived during a study conducted on the phytochemical profile and the safety of *Brassica carinata* microgreens[38]. Microgreens were grown using an innovative capillary wick irrigation system that used non-woven polyester material to facilitate water movement from the Styrofoam

boxes to the plant support medium, which was cocopeat[38]. This innovative system reduces watering frequency while maintaining standard water requirements for the microgreens[38]. Seeds weighing approximately 25 g were sown per box. The microgreens were harvested after the emergence of the first two true leaves, which occurred two weeks post-sowing (Fig. 1A). They were subsequently packaged in sterile polyethylene bags (Fig. 1B), then placed in cooler ice boxes (25 × 18 × 18 cm in dimensions) and afterward transported to the Molecular Biology and Biotechnology Laboratory at Pan African University Institute for Basic Sciences, Technology, and Innovation (PAUSTI), where they were freeze-dried at − 60 °C for 72 h (Fig. 1C), ground into a fine powder using a blender (Fig. 1D), and stored in sterile sealed bags (Fig. 1E) at 4 °C for further analysis.

Sample extraction

Aqueous extracts of *Brassica carinata* microgreens were obtained following the procedure outlined by[48] with a few modifications as follows. So, fifty (50 g) of fine powder of *B. carinata* microgreens was soaked in distilled water in a ratio of 1:10 (w/v) (Fig. 1F). The soaked plant material was shaken for 30 min at room temperature. Afterward, the resulting mixture was removed from the shaker and heated in a water bath at 60 °C for 60 min. After 60 min, the mixture was cooled at room temperature and filtered through muslin cloth and Whatman No.1 filter paper. The collected filtrates (Fig. 1G) were stored at 4 °C for subsequent investigations.

Chemicals and reagents

All chemicals and reagents were procured from accredited suppliers and complied with the highest analytical standards. Silver Nitrate was procured from Thermo Fisher Scientific, and Eagle's Minimum Essential Medium (EMEM) was purchased from Gibco BRL (Germany). Doxorubicin, MTT, and dimethyl sulfoxide (DMSO) were purchased from Solarbio Life Sciences Company, Beijing, China. Standard antibiotics and antifungals (Ciprofloxacin and Nystatin) were obtained from a Pharmaceutical Company in Nairobi, Kenya. Plates and flasks were procured from Legacy Lab Africa LTD, Nairobi, Kenya.

Pathogenic microbial strains and cell lines

Aspergillus flavus was sourced from JKUAT Laboratory of Food Sciences. While *Pseudomonas aeruginosa* ATCC 27,853, *Staphylococcus aureus* ATCC 43,300 (MRSA), *Escherichia coli* ATCC 25,922, *Klebsiella pneumoniae* ATCC 700,603, and *Candida albicans* ATCC 64,124 were provided by PAUSTI Molecular Biology and Biotechnology Laboratory. The KEMRI cell bank provided a kidney epithelial cell line derived from African green monkeys (ATCC Vero CCL-81).

Fig. 1. An illustration of plant sample collection, drying, and extraction process. (**A**) Microgreens ready to be harvested, (**B**) The microgreens were harvested and stored in a sterile bag for transport to the lab, (**C**) Microgreens freeze-dried process utilizing a freeze dryer, (**D**) Microgreens grinding using a grinder, (**E**) Microgreen powder, (**F**) Microgreen powder soaked in water for extraction, (**G**) Microgreen aqueous extract.

Isolation and identification of *aspergillus flavus* from maize samples

Aspergillus flavus was isolated using a direct plating method as previously described, with slight modifications[49]. Briefly, one gram of each maize sample was washed with distilled water, then sterilized using a sodium hypochlorite solution, and subsequently inoculated onto PDA plates supplemented with 0.1 mg of chloramphenicol to prevent bacterial contamination. The plates were kept at 28 °C for seven days, with daily monitoring. After seven days, the fungal colonies were subcultured onto fresh PDA and incubated for another seven days in order to obtain pure colonies. The morphological identification was performed through microscopic observation of the pure colonies, then further confirmed by the reverse coloration of the colonies; thus, the pure colonies were cultivated on AFPA (*Aspergillus flavus* and *Parasiticus* Agar; Hardy Diagnostics, USA) and incubated at 28 °C for 2 to 3 days[49].

Green synthesis of silver nanoparticles

The biosynthesis of AgNPs followed this approach. Briefly, 50 mL of BCME concentrated at 0.1 g/mL were mixed with 450 mL of 1 mM $AgNO_3$ solution in a 500 mL flask shielded with aluminium foil to protect the solution from sunlight. The resulting mixture was then heated at 70 °C and stirred for 1 h. After 1 h, the mixture was left at room temperature for 24 h with continuous stirring to allow the bioreduction process to complete. After 24 h, the colour change of the mixture from colourless to dark brown was the visual confirmation of the formation of AgNPs or the reduction of silver ions to AgNPs (Ag^+ to Ag^0) due to the excitation of the surface plasmon vibration[4]. The biosynthesized AgNPs were further aliquoted in 50 mL Falcon tubes and then centrifuged at 12,000 rpm for 15 min using a HERMLE Z 446 K (Germany) centrifuge. The supernatant was discarded, and the pellet was washed twice with distilled water, freeze-dried at − 60 °C, and kept at 4 °C for subsequent use.

Characterization of the synthesized AgNPs

The stability, the distribution within biological systems, the safety, and the efficacy of the nanoparticles are significantly influenced by their physicochemical properties. Therefore, in this study, the biosynthesized AgNPs were characterized using various techniques, including UV-visible spectroscopy, X-ray diffraction (XRD), Scanning Electron Microscopy (SEM), Fourier transform infrared spectroscopy (FTIR), Transmission Electron Microscopy (TEM), and Dynamic Light Scattering (DLS) Analysis.

UV-visible spectroscopy analysis

UV-Visible spectroscopy is the most relevant and straightforward method to confirm the formation of nanoparticles. Thus, the synthesis of AgNPs from the BCME was confirmed by monitoring the surface plasmonic resonance peak in a Shimadzu UV-1800 UV–Vis spectrophotometer (Shimadzu, Japan) in the range of 300 to 800[50,51]. Distilled water was used as a blank.

Fourier transform infrared spectroscopy analysis

FTIR analysis was performed to elucidate functional groups that are involved in the biosynthesis, the stabilization, and the capping processes of AgNPs. The spectral data were acquired using an IRAffinity-1 S FTIR spectrophotometer (Shimadzu Corp., 03191) equipped with an ATR. The instrument was set up to perform a total of 20 scans with 4 cm^{-1} spectral resolution for both background and sample spectra, recorded rapidly in the range between 4000 and 400 cm^{-1}. About 1 mg of the sample was loaded onto the crystal and scanned using a laser. The FTIR analysis was performed for both microgreen crude extract and synthesized *BCM*-AgNPs.

Scanning electron microscopy (SEM) and EDX analysis

The morphological analysis of AgNPs was performed using SEM according to the method outlined by[52]. The Tescan Vega 3 LMH instrument with a 20 kV accelerating voltage, a secondary electron detector (SED), and energy dispersive spectroscopy (EDS) were employed for the analysis. In order to improve conductivity, the samples were first of all coated with carbon using Agar's Turbo Carbon Coater before measurement[52].

Transmission electron microscopy (TEM) analysis

TEM analysis was carried out following the method described by[52] in order to characterize the size, shape, and morphology of synthesized AgNPs. The samples were analysed through the Jeol JEM-2100 F transmission electron microscope, which operated at 200 kV and equipped with a LaB6 source and a charge-coupled device (CCD) digital camera. Prior to performing TEM analysis, a small quantity of synthesized AgNPs was dispersed onto the TEM grid (200 mesh size Cu-grid) and subsequently coated with a thin film made of lacy carbon material[52].

Crystalline size determination using XRD

Powder XRD analysis was conducted to determine the average crystalline size of the synthesized AgNPs. The Rigaku Miniflex XRD (X-ray scientific) was used for the analysis. The Goniometer was of Bragg-Brentan geometry with a 150 mm radius and had a measurement range (2θ) of 2° – 145°. The X-ray source is a copper anode (λ Cu Kα = 1.5418 Å), I = 15 mA (fixed), U = 30 kV (fixed). Measurement speed ranged from 0.01 to 100 °/min. The samples were analysed following the manufacturer's protocol. Briefly, one to two grams of powdered synthesized AgNPs were weighed into the sample holder, and with the use of a glass slide, the sample was compacted to create an even surface area. The sample holder was then placed on the XRD multi-sample holder chamber. The machine was then calibrated (SET) accordingly to begin the analysis. The nanoparticles' crystalline size was computed using Debye Scherrer's Eq. (1), where D is the average particle size (nm), K is a constant equal to 0.94, λ is the wavelength of X-ray radiation, β is full width at half maximum of the peak in radians, and theta is the diffraction angle (degree).

$$D = \left(\frac{K\lambda}{\beta \cos \theta} \right) \quad (1)$$

Dynamic light scattering (DLS) analysis

The particle size distributions, zeta potential, and polydispersity index (PDI) of biosynthesized AgNPs were analyzed through the DLS technique, using a particle size analyzer incorporated into a computerized Malvern Zetasizer Nano system, according to the protocol described by[53]. The parameters employed for the analysis included a temperature of 25 °C, a wavelength of 633 nm, a light scattering angle of 173 degrees, a medium refractive index of 1.33, and a medium viscosity of 0.8872 cP[54].

Stability study of the synthesized AgNPs

Thermal stability of the synthesized AgNPs

About 15 mL of AgNPs suspension was aliquoted into three 15 mL Falcon tubes, each containing 5 mL of suspension. These tubes were stored at various temperatures for three months: ambient (ranging between 20 °C and 30 °C during the experiment), minus 20 °C, and minus 80 °C. Following this period, the samples were transferred from each storage location, thawed at room temperature, and their absorbance spectra were measured using a UV/Vis spectrophotometer[44].

pH stability of the synthesized AgNPs

To evaluate how the stability of the synthesized AgNPs is affected by pH, 5 mL of the synthesized AgNPs solution were allocated into five test tubes. Subsequently, each test tube containing the AgNPs was subjected to a range of pH conditions: pH 3, 5, 7, 9, and 12. The pH was adjusted by adding drops of either 1 N NaOH or 1 N HCl until the desired pH was reached, as indicated by the pH meter[55]. Following an incubation period, the UV/VIS spectrophotometer was employed to measure the absorbance spectra of the AgNPs across a scanning range of 300 to 800 nm[44].

Long-term stability of the synthesized AgNPs

The impact of Long-term storage on the stability of the synthesized AgNPs was assessed following the method described by[56] with a few modifications. Specifically, 0.5 mL of the synthesized AgNPs solution was diluted with 9.5 mL of distilled deionized water in 15 mL Falcon tubes, which were then stored in the darkness at − 20 °C for 180 days (6 months). UV-Vis spectra were measured using a spectrophotometer as follows: on day 0 (immediately post-synthesis) before storage, 45 days, 90 days, and 180 days of post-synthesis of the AgNPs.

Antimicrobial activity evaluation of *BCM*-AgNPs

Preparation of standard inocula and media

The Sabouraud Dextrose Agar (SDA), Potato Dextrose Broth (for fungi), Mueller Hinton Agar (MHA), and Mueller Hinton Broth (for bacteria) media were prepared according to the manufacturer's instructions, then sterilized by autoclaving them for 15 min at 121 °C. To obtain actively growing cultures, MHA medium was used for subculturing bacteria, while SDA medium facilitated the subculturing of fungi[57]. Standard inoculum suspensions were prepared to a turbidity equivalent to the 0.5 McFarland standard and adjusted to achieve a turbidity of 1.5×10^8 cells or spores/ml, with the turbidity verified by measuring the optical density at 600 nm[58]. Samples and standards were prepared following the methods outlined by Mwangi et al.[57] with few differences.

Antibacterial activity through the agar disc diffusion assay

The antibacterial properties of *BCM*-AgNPs against selected Gram-negative pathogens, including *E. coli*, *K. pneumoniae*, and *P. aeruginosa*, and Gram-positive pathogens, specifically *S. aureus*, were evaluated using the Kirby-Bauer disc diffusion susceptibility test as previously described by[59] with few modifications. Around 20 mL of sterile Mueller-Hinton agar was poured into each Petri dish to form a 4 mL thick plate[60]. Following the medium's cooling and solidification, the plates were inoculated by gently rubbing sterile cotton swabs that were drenched in bacterial suspensions across the whole surface[61]. To facilitate the diffusion of *BCM*-AgNPs in the inoculated media of the plates, sterile paper disks (6 mm in diameter) were loaded with 1 mg/mL of *BCM*-AgNPs solution along with negative and positive controls using a micropipette. These loaded disks were then placed onto the surface of the inoculated plates using flame-sterilized forceps. The positive control contained 1 mg/ml of ciprofloxacin, while the negative control contained 0.5% DMSO. The plates were labelled and allowed a pre-diffusion of 30 min before incubating them for 24 h at 37 °C. After incubation, the zones of inhibition around the disks, corresponding to the antibacterial activities of the tested *BCM*-AgNPs, were measured in mm[57].

Antifungal activity using the agar disc diffusion assay

Antifungal activity was investigated using two fungal species, namely *Candida albicans* and *Aspergillus flavus* on a Sabouraud Dextrose agar medium. The disk diffusion method was employed to study the antifungal activities, with nystatin as the positive control and 0.5% DMSO as the negative control. The process commenced by sterilizing the medium, followed by pouring it onto the plates to facilitate solidification. The samples, as well as positive and negative controls, were applied to the inoculated medium using the loaded disks. Following a 30 min pre-diffusion of the samples, the entire setup was incubated for 48 h at 37 °C[57]. Subsequently, the zones of inhibition were measured and recorded in mm[4].

Evaluation of minimum inhibitory concentration (MIC)

The broth microdilution assay was employed to evaluate the MIC of *BCM*-AgNPs against the tested microorganism, following the method described by[62,63] and in accordance with the guidelines of the Clinical and Laboratory Standards Institute (CLSI), standard M07-A10[64]. Briefly, 100 µL of sterile PDB (fungi) and MHB (bacteria) media were transferred into each well of a 96-well plate. Then, the *BCM*-AgNPs solutions, along with positive and negative controls, were added to the wells containing the media. Afterward, two-fold serial dilutions ranging from 1000 µg/mL to 7.81 µg/mL of the test solutions were performed[57,65]. This was followed by the inoculation in the well containing the *BCM*-AgNPs as well as positive and negative control, and subsequently, the plates were incubated at 37 °C for 24 h (bacteria) and 48 h (fungi). After 24 h and 48 h of incubation, 25 µL of the resazurin (0.15 mg/mL) was added to each well and then re-incubated for 1–2 h. The change from the blue colour of resazurin to the pink colour of resorufin indicates bacterial growth in the wells where the *BCM*-AgNPs could not inhibit growth[66]. MIC was established as the smallest concentration of AgNPs at which no observable bacterial growth was detected[67].

Determination of the minimum bactericidal (MBC) and fungicidal (MFC) concentrations

The MBC or MFC was determined using the method previously described with slight modifications[63,68] and in accordance with the CLSI guidelines. A volume of 100 µL of the bacterial and fungal suspension, which showed no bacterial or fungal growth in the MIC test, was inoculated onto MHA and SDA media and incubated at 37 °C for 24 h and 48 h, respectively, for bacteria and fungi. MBC and MFC values were defined as the lowest concentration of AgNPs at which no colony growth was observed[67].

Mode of action of AgNPs

The mechanism of action of AgNPs was identified through the MBC/MIC or MFC/MIC ratio. Antimicrobial agents with an MBC/MIC or MFC/MIC ratio < 4 are regarded as bactericidal or fungicidal, while those with an MBC/MIC or MFC/MIC ratio > 4 are termed bacteriostatic or fungistatic agents[4].

Evaluation of the safety of *BCM*-AgNPs

Cell culture conditions

The Vero CCL-81 cell line was obtained from the KEMRI cell bank and was grown in Eagle's Minimum Essential Medium (EMEM) supplemented with 10% FBS, 1% penicillin-streptomycin, 1% L-glutamine, and 1% HEPES. Cells were cultured in T75 cell culture flasks and incubated at 37 °C in 5% CO_2. The medium was changed every 48 h to allow cells to get 80% confluent.

Assessment of the safety of BCM-AgNPs using MTT cytotoxicity assay

The safety of *BCM*-AgNPs was assessed on Vero CCL-81 cells through 3-(4,5-dimethylthiazol-2-yl)-2,5-diphenyltetrazolium bromide (MTT) assay. MTT assay determines the metabolic activity of the mitochondria of the viable cells by measuring their ability to reduce MTT to formazan using the succinate-tetrazolium reductase system[69]. Vero CCL-81 cells at 80–90% confluence were subjected to two rounds of washing with 8 mL of phosphate-buffered saline (PBS). Subsequently, 1 mL of 0.25% trypsin-EDTA was used to detach the cells, followed by an incubation period of 3–4 min. Afterward, the cells were counted using a hemocytometer, and after staining them with 0.4% trypan blue, the resulting suspended cells were then seeded into 96-well plates at a concentration of 1×10^4 cells in 100 µL of growth medium per well. The plates were then incubated at 37 °C with 5% CO_2 for 24 h to facilitate the cell attachment. Following the 24 h period of incubation, the initial seeding medium was removed from the well, and 100 µL of a new medium containing various working concentrations of AgNPs (500 µg/mL, 250 µg/mL, 125 µg/mL, 62.5 µg/mL, and 31.25 µg/mL, 15.62 µg/mL, 7.81 µg/mL) was added. Dimethyl sulphoxide (0.2% DMSO) was used as a negative control and doxorubicin as positive control. The cells subjected to treatment were then incubated under the previously mentioned conditions for 24 h[70]. After that, the medium with AgNPs was removed and was added 100 µL medium with 10 µL of freshly prepared MTT solution (at a concentration of 5 mg/mL) in each well, and the plates were further incubated for 4 h. Subsequently, the MTT solution was removed, and 100 mL of 100% DMSO was added to dissolve the formazan crystals. The absorbance at 570 nm was then measured using an ELISA plate reader (an Infinite M1000 by Tecan). Each experiment was conducted in triplicate. The percentage of cell viability was computed using the formula (2)[71].

$$(\%)\ \text{Cell viability} = \frac{(\text{Abs of treated cell} - \text{Abs blank})}{(\text{Abs of untreated cells} - \text{Abs blank})} \times 100 \quad (2)$$

Statistical analysis

All experiments were carried out in triplicate, and data were analysed as the mean ± SD. Statistical significance was assessed through Origin Lab Pro (2024) using one-way ANOVA followed by Turkey's test, and a *P*-value of ≤ 0.05 was considered statistically significant. IC50 values were computed, and all analyses of cell culture data were conducted using GraphPad Prism 8. The XRD analysis was performed using Origin Lab Pro (2024) software.

Ethical statement

The use of this plant species for experimental purposes does not require any special permit. All methods used in this study comply with relevant institutional, national, and international guidelines and regulations.

Results

Characterization of synthesized AgNPs

When BCME was mixed with $AgNO_3$ (Fig. 2), the colour changed from colourless to dark brown, was a visual indicative of the formation of *BCM*-AgNPs (Fig. 2).

UV-visible spectroscopy analysis

The spectrum depicted in (Fig. 3) exhibited a maximum absorption peak of *BCM*-AgNPs at a wavelength of 420 nm, which falls within the range of surface plasmon resonance (SPR) for AgNPs, reported to range from 400 to 450 nm[44].

Fourier transform infrared spectroscopy (FTIR)

Figure 4 compares the FTIR pattern of BCME and *BCM*-AgNPs obtained using an FTIR spectrometer within the range of 400–4000 cm^{-1}. Various vibrational frequencies were identified, indicating the existence of diverse biological functional groups involved in the reduction and stabilization process during the biosynthesis of AgNPs. The IR pattern of BCME revealed the presence of several peaks at 3267, 3027, 1745, 1582, 1375, 1080, and 522 cm^{-1} while the IR pattern of *BCM*-AgNPs displayed prominent picks at 3254, 3020, 1739, 1576, 1360 cm^{-1}. The peaks at 3267 and 3027 cm^{-1} are assigned to the O-H stretching vibration of carboxylic acid groups, illustrating the existence of phenols and flavonoids[72,73]. Peaks at 1739 and 1576 cm^{-1} in the IR spectra are attributed to the carbonyl stretch of the amide-I bond and the -N-H stretch vibrations of the amide-II bond, confirming the occurrence of proteins[74]. The peak at 1375 cm^{-1} is due to C-H asymmetrical stretching of alkanes. The peak at 1080 cm^{-1} is caused by carboxylic acid C-OH stretching, whereas peaks at 522 cm^{-1} show phenol group O-H stretching[73]. The comparison between the FT-IR spectra of BCME and those of AgNPs revealed notable differences. Indeed, some peaks were displaced, while the intensity of other peaks decreased or increased. For instance, the peaks at 3267, 3027, 1745, 1582, and 1375 assigned to O–H and N–H stretching vibrations cm^{-1} observed in the IR of BCME were moved to 3254, 3020, 1739, 1576, and 1360 cm^{-1}, respectively, in the IR of *BCM*-AgNPs. This may be owing to electrostatic interactions among AgNPs and capping agents contained in the extract[75].

Scanning electron microscopy and EDX analysis

Figure 5A shows the nearly spherical form and smooth, even texture of the synthesized AgNPs, while (Fig. 5B) displays the EDX spectra, indicating the presence of elements such as Ag, Cl, C, O, and S. Moreover, the quantitative EDX analysis revealed a 72% predominance of the Ag element in AgNPs derived from *Brassica carinata* microgreen.

Transmission electron microscopy analysis

Figure 6A–C displays TEM micrographs of the biosynthesized AgNPs taken at different levels of resolution, while (Fig. 6D) presents the size distribution histogram of *BCM*-AgNPs. The TEM micrographs unveiled a well-distributed, crystalline structure and roughly spherical shape of biosynthesized AgNPs. The particle size analysis conducted using ImageJ software indicated that the size of the AgNPs ranged from 22.36 to 48.55 nm, with an average size of 34.68 nm (Fig. 6D).

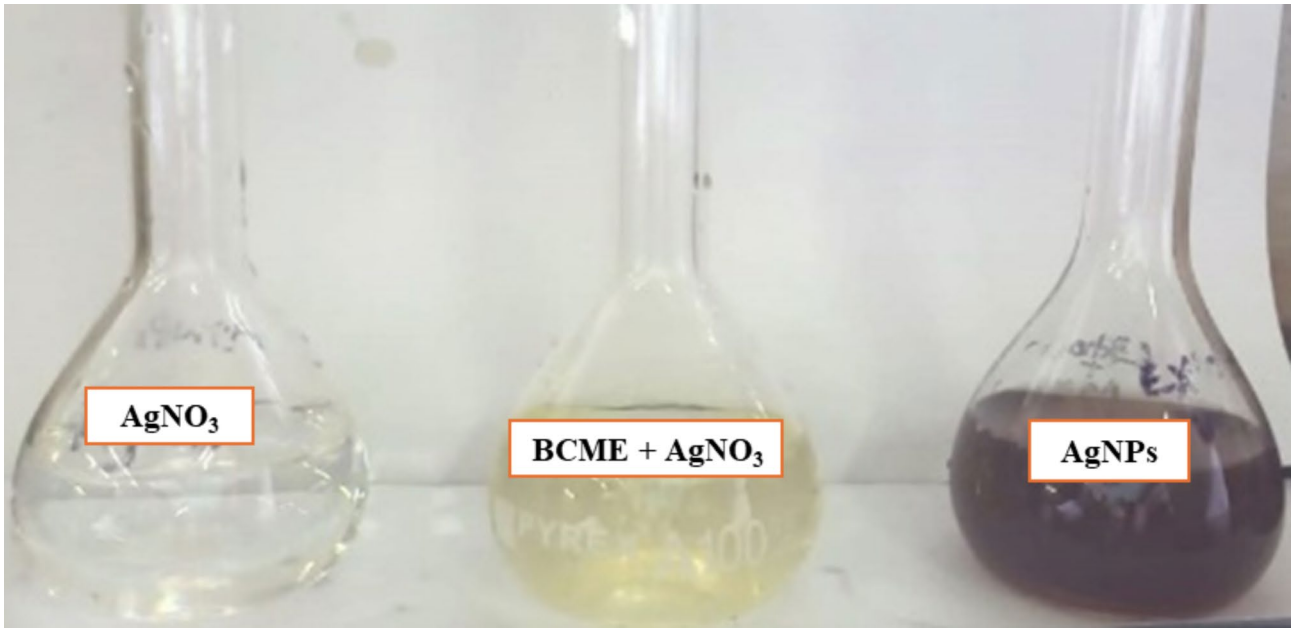

Fig. 2. Evidence of colour change during biosynthesis of AgNPs.

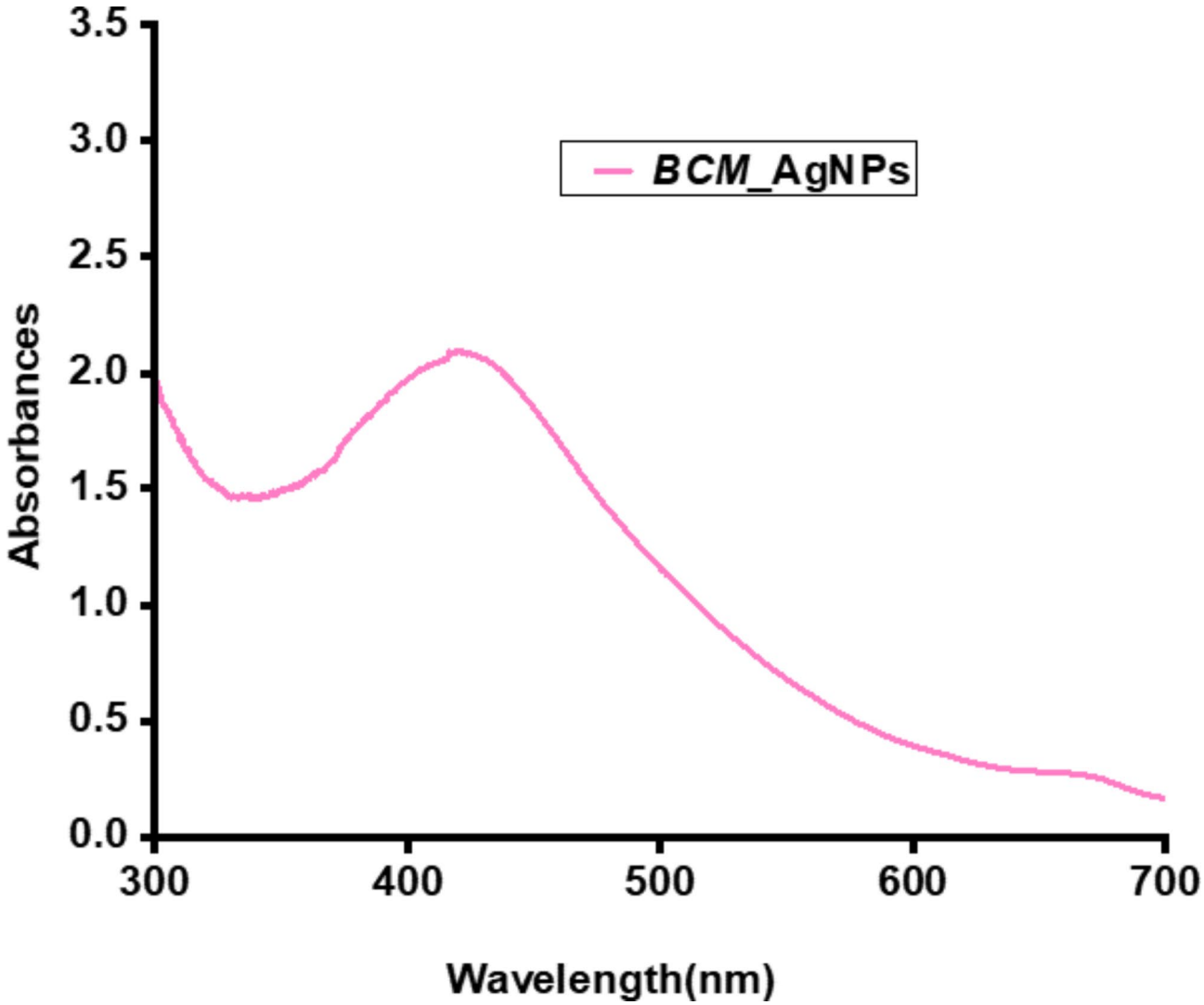

Fig. 3. UV/VIS spectra of *BCM*-AgNPs.

Crystalline size determination using XRD

Figure 7 shows the XRD pattern of biosynthesized AgNPs mediated by BCME. Characteristic diffraction peaks were detected at the angles of 28.1°, 32.49°, 38.3°, 46.45°, 55°, and 57.8°. The presence of diffraction peaks centred at angles 2θ of 38.3°, 46.45° and 55° corresponding to the (111), (200), and (220) reflection planes, respectively, indicates the face-centred spherical structure of silver. The average size of the AgNPs generated by bioreduction was computed using the Scherrer Eq. (1), and approximately 22.88 nm was found to be the average diameter of the biosynthesized AgNPs.

Dynamic light scattering analysis

Figure 8 exhibits the DLS analysis, indicating that the average size of AgNPs particles is 196.4 ± 2.12 nm and their polydispersity index is 0.13 ± 0.02. Meanwhile, Fig. 9 illustrates the zeta potential of AgNPs, estimated at -22.5 ± 1.16 mV.

Stability study of the synthesized AgNPs

Thermal stability of the synthesized AgNPs

Figure 10 shows that the AgNPs remained stable throughout all tested temperatures, with a characteristic absorption peak ranging from about 420 nm to 430 nm, which is well within the range of AgNPs.

PH stability of the synthesized AgNPs

Figure 11 indicates that the AgNPs remained stable under all tested pH values, with a typical absorption peak between about 420 nm and 450 nm, which falls within the range of AgNPs.

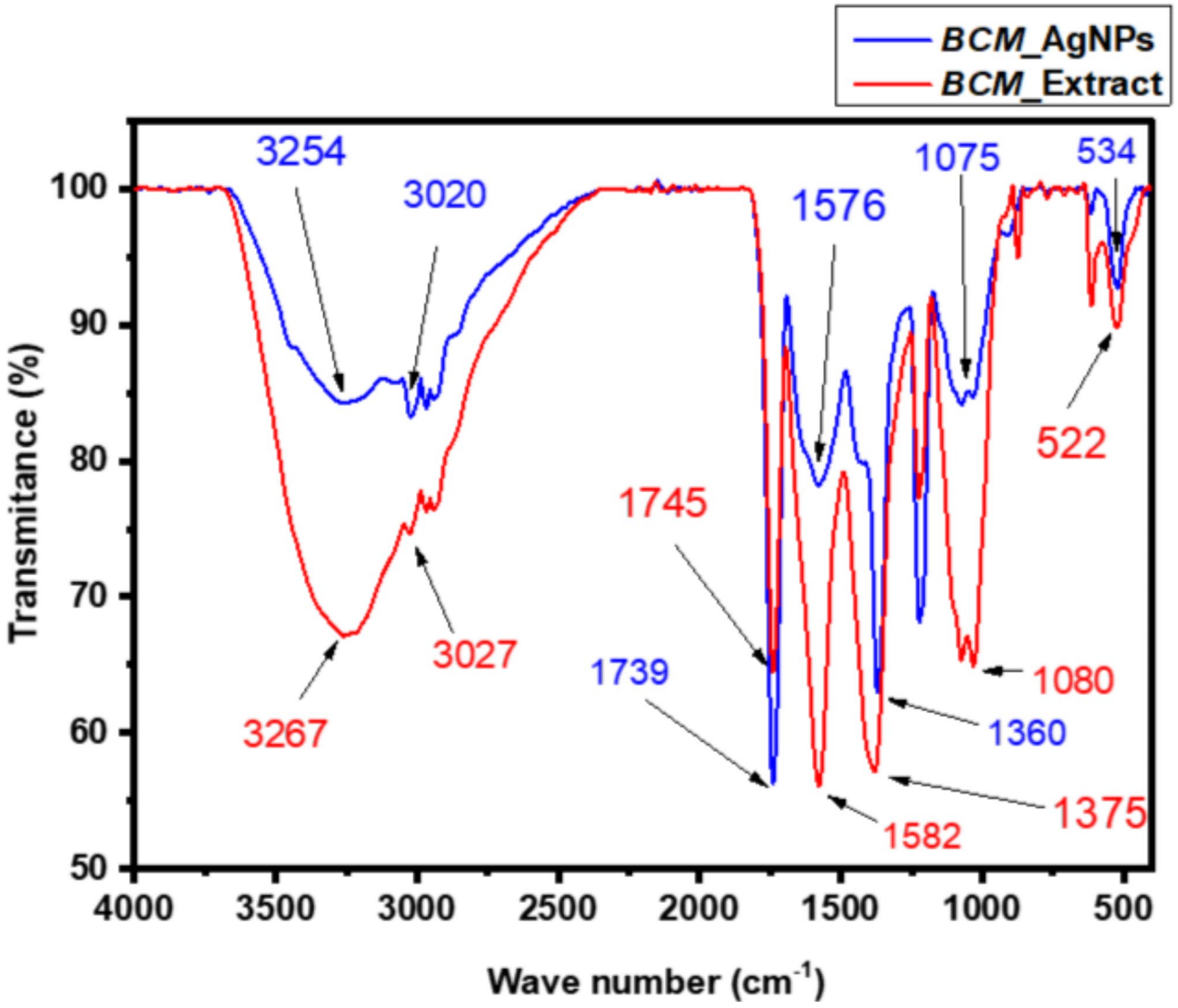

Fig. 4. FT-IR spectra of *BCM*-AgNPs and microgreen extrac.

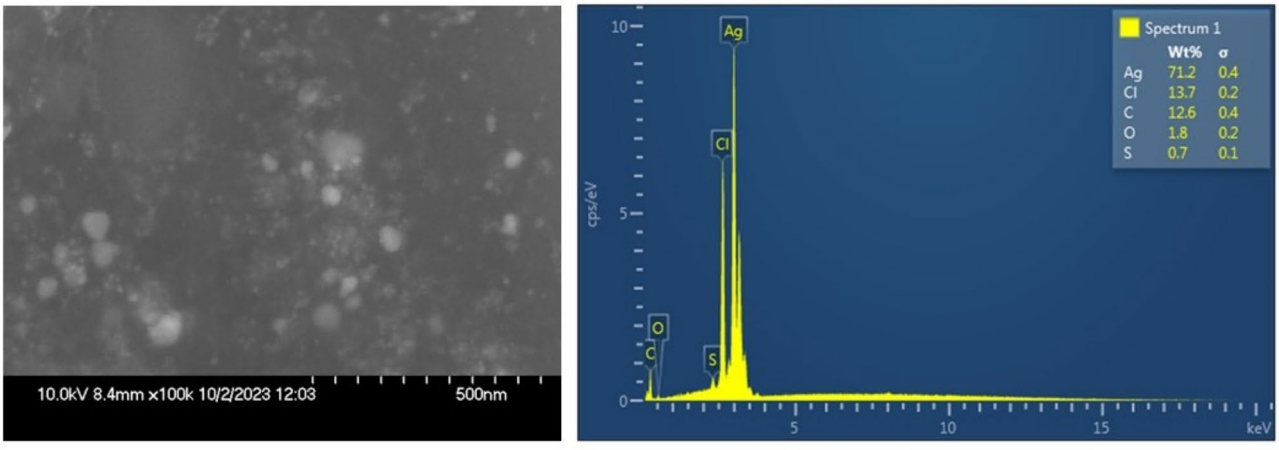

Fig. 5. (**A**) SEM micrograph showing the morphology of *BCM*-AgNPs. (**B**) EDX spectra showing the amounts of different elements present in the biosynthesized *BCM*-AgNPs.

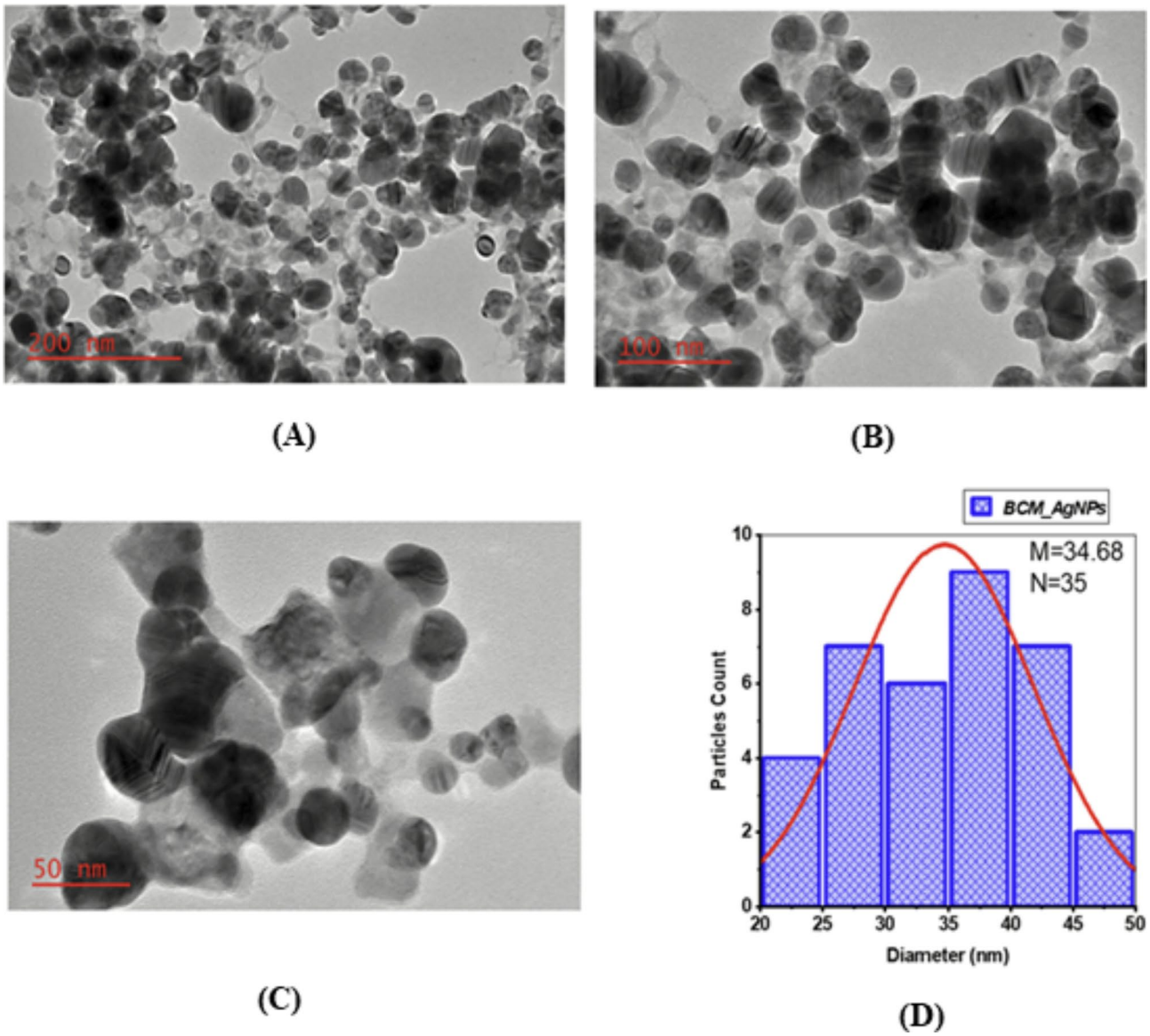

Fig. 6. (**A**–**C**) TEM micrographs of the *BCM*-AgNPs at different resolutions. (**D**) Shows particle size distribution histogram of *BCM*-AgNPs.

Storage stability of the synthesized AgNPs

Figure 12A–D depicts the stability of biosynthesized AgNPs over long-term storage. The result demonstrated that the combination of darkness and low temperature has a crucial influence on the stability of AgNPs, thereby ensuring their better long-term stability.

Antimicrobial activity evaluation of *BCM*-AgNPs

Inhibitory activity of BCM-AgNPs

Figure 13A–F shows the results of the antimicrobial activity of *BCM*-AgNPs, along with the negative and positive controls, against six selected pathogens. The results are presented as zones of inhibition.

In this study, the antimicrobial potential of *BCM*-AgNPs was evident through remarkable zones of inhibition observed against the microorganism under investigation, as depicted in (Fig. 13) and detailed in Table 1. The susceptibility of microorganisms to *BCM*-AgNPs was classified as follows: lack of activity, represented by zones of inhibition 0–7 mm; moderate activity, indicated by zones of inhibition 8–12 mm; and promising activity, observed in zones of inhibition 12 mm and above[4]. Based on this classification, it is evident that *BCM*-AgNPs showed potent antimicrobial activity against all the pathogen strains tested. *A. flavus*, *S. aureus*, and *K. pneumoniae* exhibited the highest sensitivity to *BCM*-AgNPs, with IZD of 28.33, 21.53, and 20.14, respectively. On the other hand, *E. coli*, *P. aeruginosa*, and *C. albicans* have demonstrated good sensitivity to *BCM*-AgNPs, with IZD of 16.23, 17.20, and 18.43, respectively. The finding revealed a significant difference in the zones of inhibition values for the standards and the *BCM*-AgNPs ($P < 0.05$).

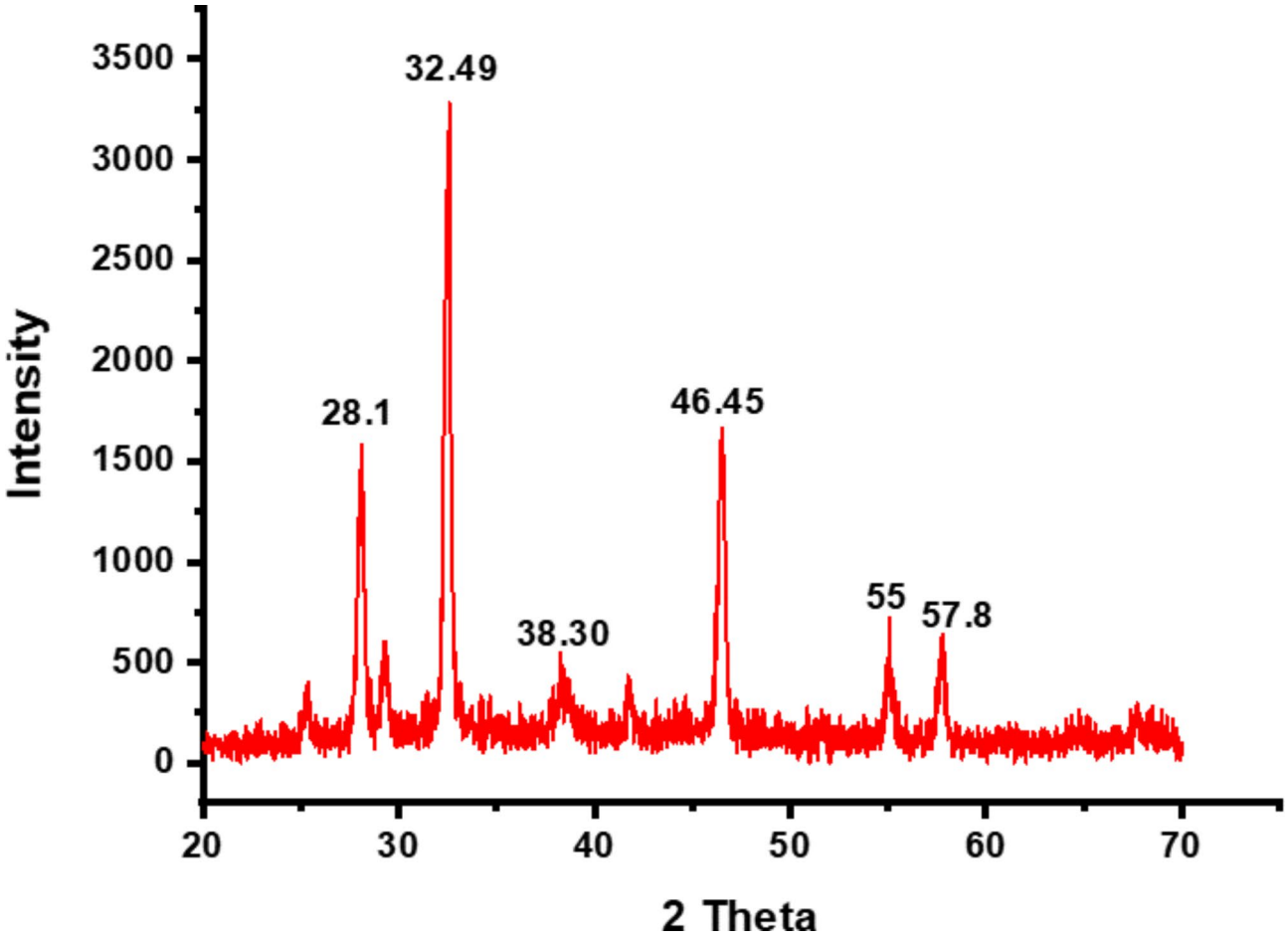

Fig. 7. X-ray diffractogram of biosynthesized *BCM*-AgNPs.

Evaluation of minimum inhibitory concentration (MIC) of BCM-AgNPs

Table 2 shows the minimum inhibitory concentration (MIC) values of *BCM*-AgNPs against tested pathogens. The lowest MIC value was observed in *P. aeruginosa* (62.5 µg/mL), followed by those observed in *A. flavus* (125 µg/mL), *E. coli* (125 µg/mL), and *S. aureus* (250 µg/mL), indicating that *BCM*-AgNPS exhibits antimicrobial properties at low concentrations. The percentage of spectrum activity measures the effectiveness of an antimicrobial agent against a range of microorganisms. It is computed by dividing the number of sensitive strains by the total number of strains tested and multiplying by 100. This percentage reflects the breadth of the antimicrobial's effectiveness, with a higher percentage indicating a broader spectrum of activity against various pathogens[67]. *BCM*-AgNPs exhibited a 100% antimicrobial activity spectrum against all tested microbial strains at concentrations ranging from 1000 µg/mL to 250 µg/mL and a 50% activity spectrum at 125 µg/mL. Our findings indicate that AgNPs have the potential to be antibacterial agents against a broad spectrum of pathogenic strains, with antimicrobial effectiveness dependent on AgNPs concentration, and are in line with those of previous studies[67]. The percentage of spectrum activity was computed using the formula below:

$$(\%)\ \text{spectrum activity} = \frac{(\text{Number of pathogens inhibited})}{(\text{Total Number of pathogens tested})} \times 100 \quad (3)$$

Determination of minimum bactericidal or fungicidal concentration (MBC or MFC) of BCM-AgNPs

Table 3 depicts the MBC and MFC of *BCM*-AgNPs. The MBC value for *P. aeruginosa* and the MFC value for *A. flavus* were both 125 µg/mL. The MBC was 250 µg/mL for *S. aureus*, and *E. coli*. It was 500 µg/mL for *K. pneumoniae*; on the other hand, *C. Albicans* had an MFC of 500 µg/mL. The findings indicate that *BMC*-AgNPs have 100% antimicrobial spectrum activity at concentrations of 1000 µg/mL and 500 µg/mL. The activity spectrum was 66.66% and 33.33% at concentrations of 250 µg/mL and 125 µg/mL, respectively. Nevertheless, the antibacterial activity spectrum was null at 62.5–7.81 µg/mL.

Mode of action of BCM-AgNPs

The mechanism by which *BCM*-AgNPs act against the tested pathogenic strains is detailed in Table 4. The results revealed that *BCM-AgNPs* exhibited both bactericidal and fungicidal effects, with MBC/MIC or MFC/

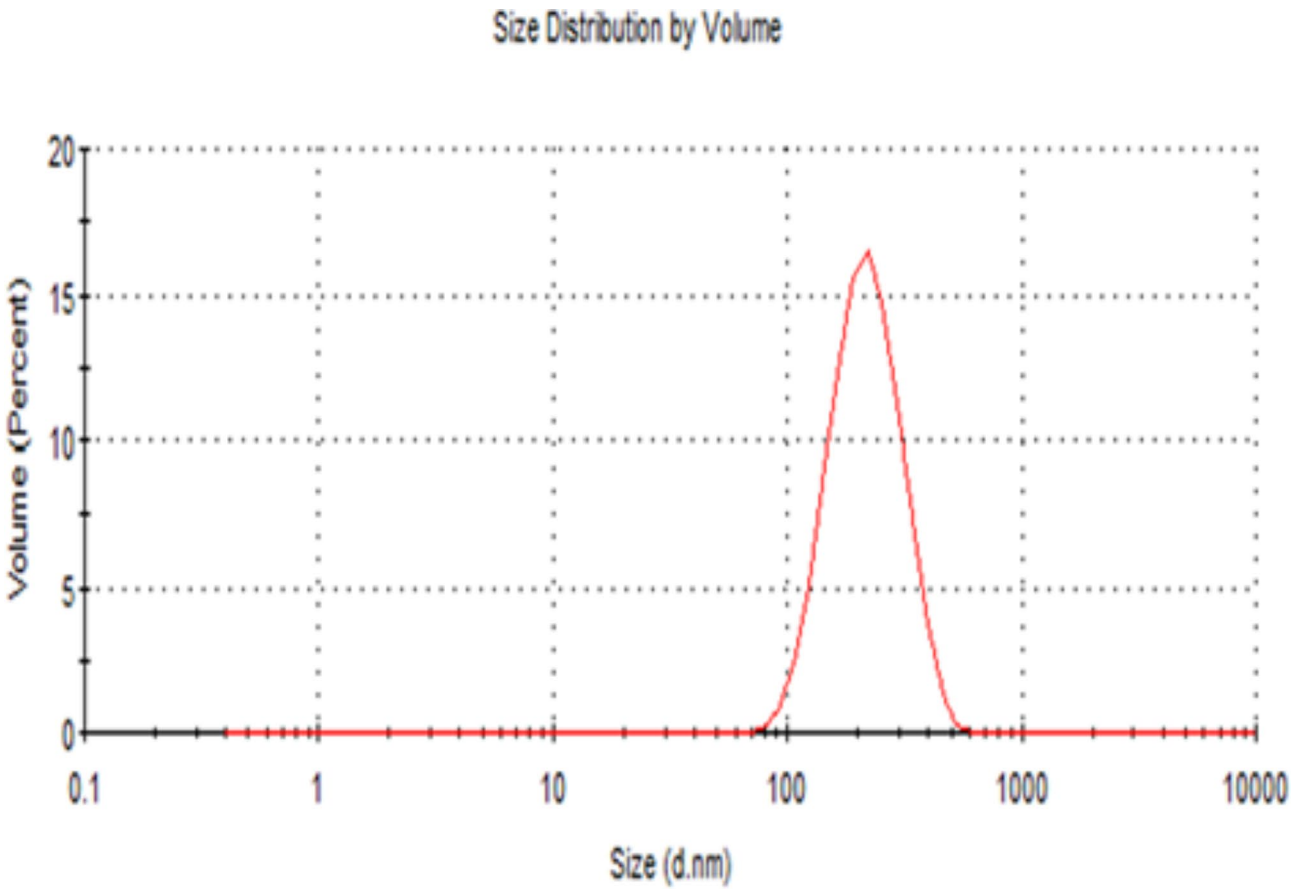

Fig. 8. DLS analysis of particle size and distribution.

MIC ratios ≤ 4 for all pathogenic strains assessed[4]. Thus, the biosynthesized *BCM*-AgNPs act bactericidally and fungicidally on both Gram-positive and Gram-negative bacteria as well as fungi.

Assessment of the safety of *BCM*-AgNPs using MTT cytotoxicity assay

Figure 14 depicts the viability percentage of Vero normal cells at various concentrations of *BCM*-AgNPs. The results indicate that the viability of Vero cells decreased as the concentration of *BCM*-AgNPs increased. On the other hand, the half-maximal inhibitory concentration (IC50) was found to be 152.4 µg/mL, highlighting its safety.

Figure 15 shows the results of the Cytotoxicity of *BCM*-AgNPs on Vero cell line. Well 1–11 from row A-G contained Vero cells. Well 1–4 from row A-G, contained 500 µg/mL, 250 µg/ mL, 125 µg/ mL, 62.5 µg/ mL,31.25 µg/ mL, 15.62 µg/ mL, 7.81 µg/ mL of *BCM*-AgNPs solution respectively. Well 5–7 from row A-G contained a negative control (DMSO 0.2%). Well 8–11 from row A-G contained a positive control (Doxorubicin). Row H and column 12 contained the blank.

Discussion

Drug resistance has increased dramatically in recent decades, posing a serious threat to global public health. Most antibiotics have become ineffective due to microbial resistance[76]. Therefore, finding new alternatives has become vital to addressing this significant issue. The use of plant secondary metabolites for synthesizing AgNPs appears to offer a more promising solution[77]. In this study, BCME was employed to synthesize *BCM*-AgNPs. Various analyses were conducted in order to assess the successful synthesis of the *BCM*-AgNPs. These encompassed observing colour changes visually and scrutinizing the physical and chemical properties attributed to the biosynthesized AgNPs through spectroscopy and microscopy techniques.

In solution, the AgNPs exhibit a dark brown colour owing to the excitation of their surface plasmon resonance (SPR)[44,78]. This study validated the formation of AgNPs by observing the change in colour of the mixture from colourless to dark brown. The findings align with earlier research[4,78].

UV-Vis spectroscopy is essential for detecting the synthesis of AgNPs by observing their electronic structures and optical properties. When AgNPs form, electron clouds oscillate on their surface, absorbing specific frequencies of electromagnetic waves. This phenomenon, called surface plasmon resonance (SPR), is characteristic of AgNPs and is detected using a UV-Vis spectrophotometer[79–81]. AgNPs biosynthesized mediated by BCME exhibited a UV/VIS absorption spectrum at 420 nm (Fig. 3), in alignment with the surface plasmon resonance of AgNPs[82]. This finding is consistent with previous studies on the synthesis of AgNPs using plant

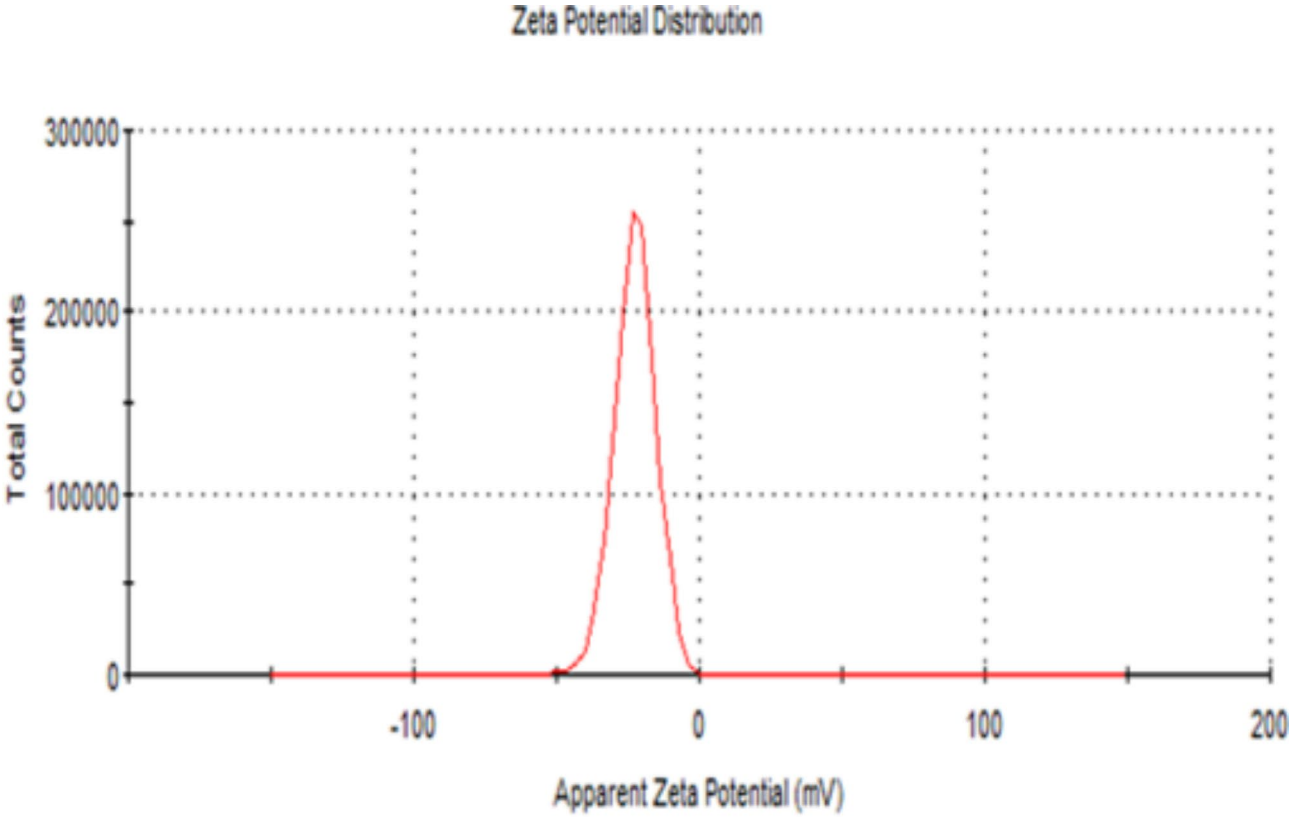

Fig. 9. Zeta potential analysis of *BCM*-AgNPs.

extracts[4]. Several studies have shown the synthesis of AgNPs exhibiting UV/VIS absorption peaks at 413 nm[31], at 420 nm[82,83], at 435 nm[55,84], and others at 450 nm[85]. The results demonstrate the potential for easy and eco-friendly synthesis of AgNPs using BCME.

To investigate the process of $AgNO_3$ reduction by BCME in the biosynthesis of AgNPs, FTIR analysis was performed to elucidate the potential interactions between silver salts and the phytochemicals involved in the reduction of Ag^+ ions to Ag^0 and the stabilization of synthesized AgNPs. Figure 4 depicts the IR spectra of BCME and the synthesized *BCM*-AgNPs. The characteristic peaks from FTIR analysis were identified by comparing them with the FT-IR data from other studies on the synthesis of AgNPs using green methods[75]. The comparative analysis of the FTIR spectra of BCME and *BCM*-AgNPs indicated that the biomolecules present in the BCME have fundamentally contributed to the formation of *BCM*-AgNPs. The heightened intensity of the peak at 1745 cm^{-1} observed in the FT-IR spectrum of the *BCM*-AgNPs, associated with carbonyl vibrations, implies that the reduction of silver ions is a result of the conversion of hydroxyl groups to carbonyl groups within the plant extract[75]. In addition, the decrease in the intensity of the peaks at 3254 and 3020 cm^{-1} in the IR spectrum of AgNPs indicates the crucial role of O-H and N-H groups in the reduction process and bond formation mechanism throughout AgNPs biosynthesis[86]. The presence of specific absorption peaks indicated the existence of phytochemicals, such as amino acids, carbohydrates, phenols, flavonoids, and alkaloids, on the surface of nanoparticles that were responsible for capping and stabilizing AgNPs. This helped to prevent the particles from aggregating. The biomolecules involved in this process played a crucial role in ensuring the efficient stabilization of AgNPs[73,87]. Our results align with prior studies conducted on AgNPs biosynthesis[73,88].

SEM analysis (Fig. 5A) revealed the spherical shape and smooth texture of the synthesized AgNPs. These findings are consistent with the UV-visible spectrum, which showed maximum absorption at 420 nm[44,82]. Previous studies have reported various forms of AgNPs, including the spherical form[89–91]. The spherical AgNPs obtained in this study are thus compatible with the expected silver nanoparticle morphologies.

EDX spectra (Fig. 5B) revealed the presence of various elements in the biosynthesized AgNPs, with silver (Ag) being the most abundant element, accounting for 72%, as evidenced by the presence of a prominent peak in the spectra. These findings suggest a high level of purity in the biosynthesized AgNPs and align with previous studies[44]. The other minor peaks indicate the presence of contaminants at low concentrations, likely due to environmental factors during synthesis and pre-experimental procedures, such as gold coating and the use of glass slides. Additionally, residual phytochemicals from the plant extract used in the synthesis process may also contribute to the observed contaminants[92–95]. The crystalline and spherical nature of the well-distributed AgNPs were further confirmed by TEM analysis (Fig. 6A–C). The average particle size was found to be 34.68 nm (Fig. 6D), which is consistent with the size obtained by XRD analysis. These findings align with those reported in previous studies[96,97].

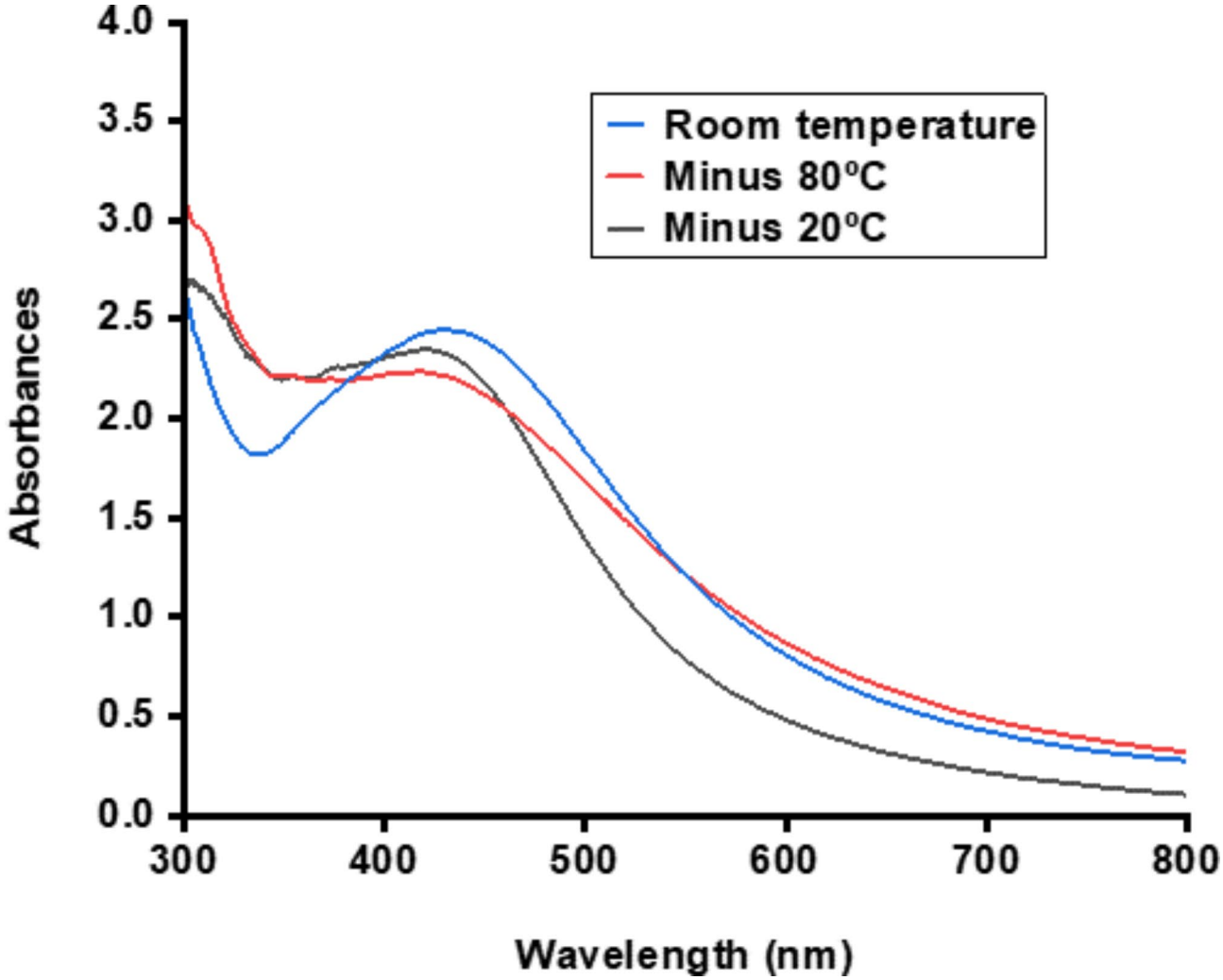

Fig. 10. UV/VIS spectra revealing the temperature stability of synthesized AgNPs.

XRD analysis confirmed the crystalline nature of the AgNPs, as evidenced by the presence of diffraction peaks centred at 2θ angles of 38.3°, 46.45°, and 55° (Fig. 7) corresponding to the (111), (200), and (220) reflection planes, respectively, indicating the face-centred spherical structure of silver, as indexed in Joint Committee on Powder Diffraction Standards (JCPDS) file no. 84–0713 and 04–0783 and reported by previous studies[98–100]. However, the additional peaks observed at 28.1°, 32.49°, and 57.8° correspond to AgCl (111), (200), and (202) planes, respectively, which could be due to the presence of chloride ions in the aqueous extracts, leading to the formation of both AgCl and Ag[101,102]. Pure AgNPs are inherently unstable in environmental conditions and tend to react with inorganic ligands, such as sulphide and chloride, when silver is oxidized. The plant extracts used in the synthesis of AgNPs contain chloride ions, which are among the most prevalent monovalent ions in natural aqueous systems[59,103]. Therefore, during the synthesis of AgNPs using these extracts, a reaction between chloride ions and silver ions occurs, leading to the simultaneous formation of AgCl and AgNPs, thereby accounting for their presence in the XRD profile[59]. Moreover, the Peak at 2θ value 32.49° has recorded the highest intensity, which is consistent with findings from prior research. Actually, the peak at 32.49° appears whenever there is a large amount of silver oxide nanoparticles; this sharp distinct peak shows that silver is a primary component in the synthesis[104,105]. The XRD findings revealed that the biosynthesis process generated AgNPs with an average size estimated at 22.88 nm. TEM analyses provided further evidence of the crystalline nature and spherical morphology of these AgNPs. Furthermore, the average particle size determined by TEM was approximately 34.68 nm, which was relatively close to that obtained by XRD (22.88 nm).

The DLS method relies on light interacting with particles and is used to analyse size distributions of small particles ranging from 2 to 500 nm[106,107]. DLS analysis revealed larger AgNPs sizes (196.4 nm) (Fig. 8) compared to those reported by XRD (22.88 nm) and TEM (34.68 nm). This significant difference between the DLS values and those from TEM and XRD has been reported in previous studies[44], and could be attributed to the fact that the size measured by DLS is a combination of the particles and the hydrodynamic radius, which does not represent the actual size of the AgNPs due to the presence of a hydration layer around the AgNPs and coatings[44,108,109].

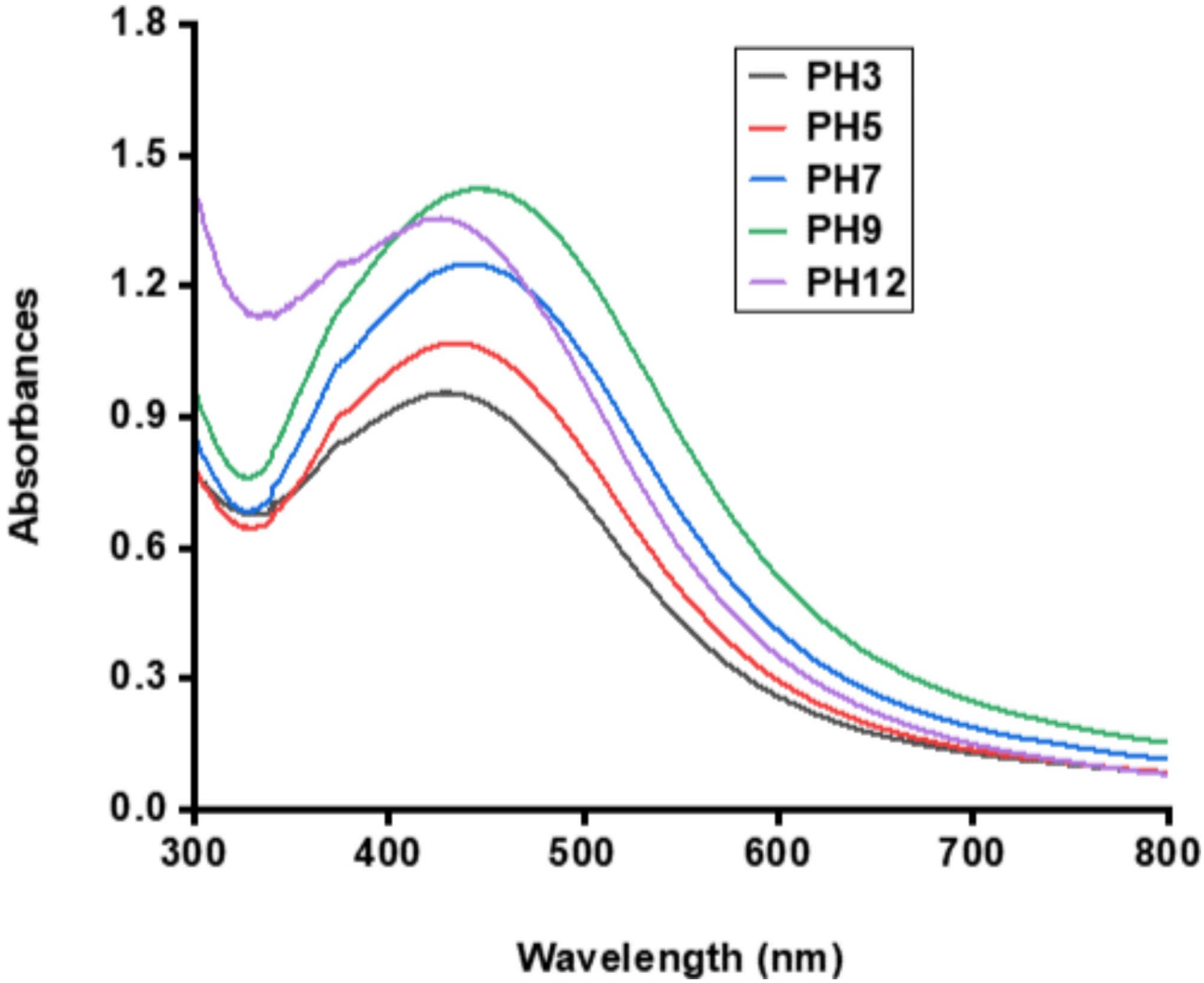

Fig. 11. UV/VIS spectra exhibit the pH stability of synthesized AgNPs.

The polydispersity index (PDI) measures the heterogeneity of a sample based on size. A smaller PDI indicates greater homogeneity[110]. Nanoparticles with a PDI of less than 0.3 are considered suitable for drug delivery[109,111,112]. The synthesized AgNPs had an average PDI of 0.13 ± 0.02, emphasizing their high uniformity and indicating their potential effectiveness across various fields, particularly in the medical field[44].

The zeta potential is the potential difference between the surface of suspended nanoparticles and the surrounding liquid. This parameter reflects the particle charge, indicating the potential stability of the colloidal system[113,114]. The zeta potential of the biosynthesized *BCM*-AgNPs was found to be -22.5 ± 1.16 mV (Fig. 9). The AgNPs synthesized using BCME are, therefore, stable due to significant zeta potential, which prevents the flocculation of AgNPs[113,115].

The stability of a substance under various conditions has a significant impact on its relevance and applicability. We investigated the stability of biosynthesized AgNPs under different temperatures, pH levels, and long-term storage. Figure 10 shows that the AgNPs remained stable throughout all tested temperatures, with a characteristic absorption peak ranging from about 420 nm to 430 nm, which is well within the range of AgNPs[55,89,116]. This indicates that the AgNPs remain effective under different temperatures[44]. Regarding pH stability, the results reveal that the AgNPs remained stable under all pH values tested, with a characteristic absorption maximum between 420 nm and 450 nm (Fig. 11), which falls within the range of AgNPs[55,89,116]. This stability is vital as it demonstrates that AgNPs can maintain their effectiveness in varying pH conditions, such as those found in the gastrointestinal tract. This property is essential for ensuring the efficacy of AgNPs. It helps to prevent a common issue encountered with many plant extracts, which often lose their effectiveness in vivo due to pH variations[46]. Figure 12A–D presents the results of the stability test of biosynthesized AgNPs under long-term storage. The biosynthesized *BCM*-AgNPs exhibited the characteristic SPR peak ranging from 416 to 430 nm, which is within the range of AgNPs[117]. This suggests that the AgNPs remained stable even after six months of storage, as they maintained their characteristic SPR peaks, indicating that they preserved their inherent properties as AgNPs. This stability is highly favourable and practical for nanoparticle synthesis. Moreover, the sustained stability of

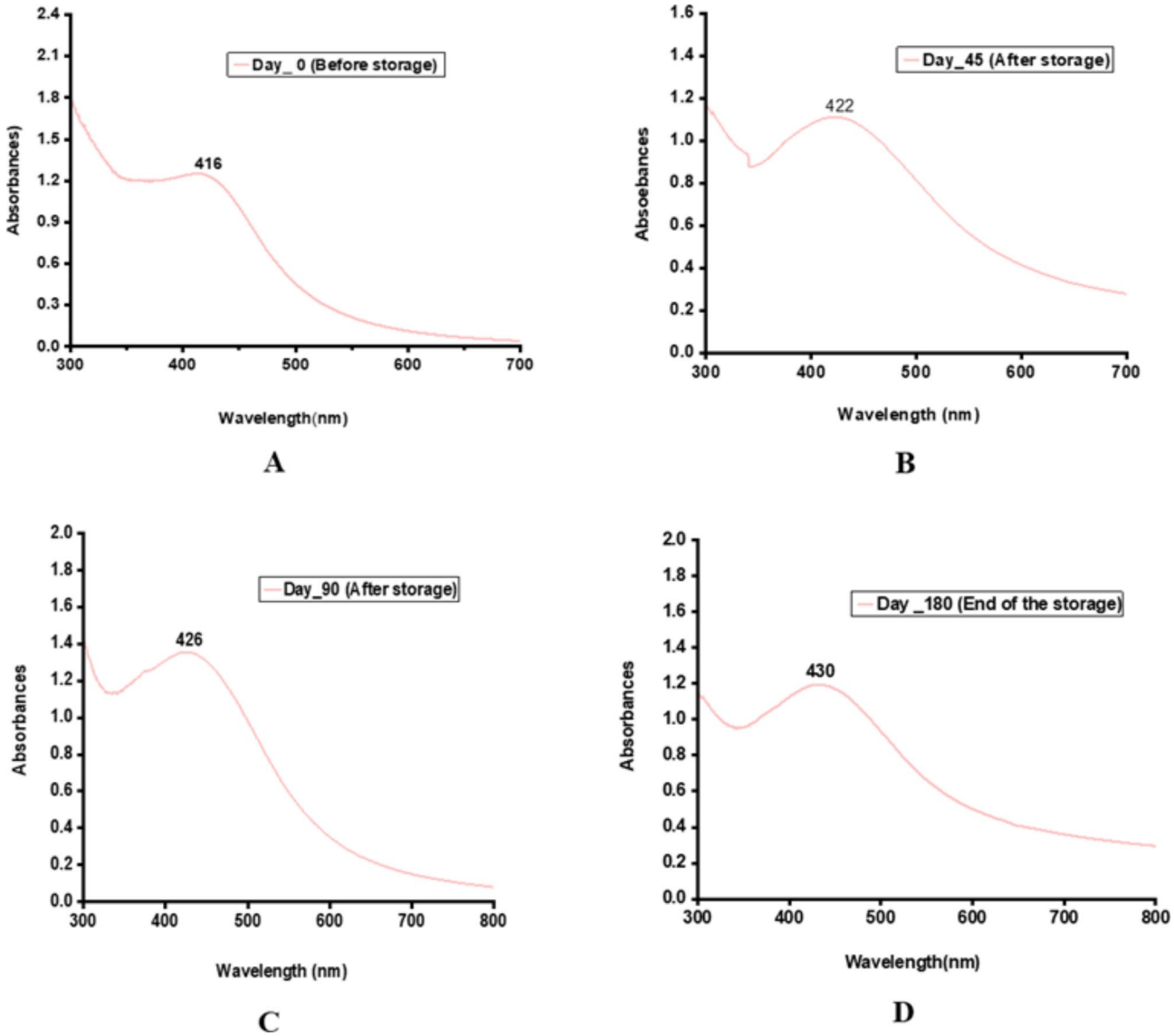

Fig. 12. UV/VIS spectra indicating the storage stability of synthesized AgNPs.

the AgNPs suggests that their application is both potent and long-lasting[118]. Additionally, the findings indicate that *BCM*-AgNPs stored in darkness and at low temperatures maintain their stability after six months, which is consistent with previous studies[119]. The increase in the absorption peak of *BCM*-AgNPs from 416 nm on day 0 to 430 nm on day 180 could be attributed to slight aggregation during storage as the duration increases. However, these aggregations are negligible, as they did not result in the loss of the intrinsic properties of AgNPs, which is their characteristic absorption peak between 400 and 450 nm. Further instruments, such as SEM, DLS, TEM, and XRD, are necessary for a more precise and relevant evaluation of the future *BCM*-AgNPs' stability.

Many studies have highlighted the antimicrobial potency of biosynthesized AgNPs against a broad array of pathogens, including those resistant to standard antibiotics. This effectiveness is attributed to the unique mechanism of action of AgNPs, which plays a crucial role in preventing the emergence of antimicrobial resistance[120,121].

This study investigated the antimicrobial activity of biosynthesized AgNPs. The findings demonstrate the potent antimicrobial activity of biosynthesized *BCM*-AgNPs against a wide range of microbial pathogens, including fungi and both gram-positive and gram-negative bacteria, as shown in (Table 1). These results concur with the findings of the previous studies that have proven both the antifungal efficacy and antibacterial properties of biosynthesized AgNPs[121–124].

The susceptibility of microorganisms to *BCM*-AgNPs was categorized as follows: no activity (0–7 mm zone of inhibition), moderate activity (8–12 mm), and strong activity (≥ 12 mm). According to this classification, *BCM*-AgNPs exhibited promising antimicrobial activity against all tested pathogen strains. *A. flavus*, *S. aureus*, and *K. pneumoniae* have exhibited the highest sensitivity to *BCM*-AgNPs, with IZD of 28.33, 21.53, and 20.14 mm, respectively. On the other hand, *E. coli*, *P. aeruginosa*, and *C. albicans* have shown good sensitivity to *BCM*-

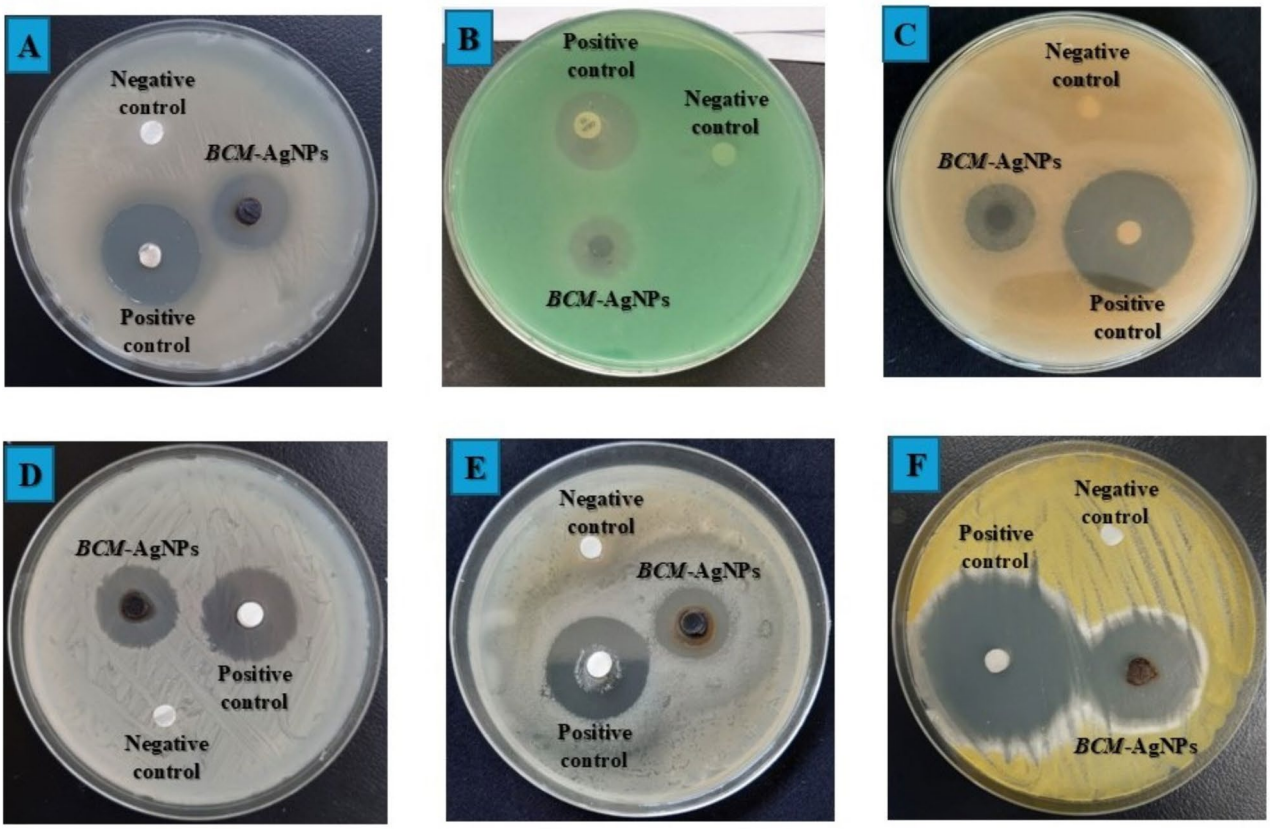

Fig. 13. Antimicrobial potential of biosynthesized *BCM*-AgNPs against selected pathogens. (**A**) *S. aureus*, (**B**) *P. aeruginosa*, (**C**) *E. coli*, (**D**) *C. albicans*, (**E**) *K. pneumonia*, *and* (**F**) *A. flavus.*

Microorganism	IZD (Mean ± SD mm)	
	Standards (1000 µg/mL)	AgNPs (1000 µg/mL)
Gram positive bacterium		
S. aureus	26.66 ± 0.57^{bc}	21.53 ± 0.50^{d}
Gram negative bacteria		
E. coli	25.96 ± 0.05^{c}	16.23 ± 0.68^{g}
K. pneumoniae	28.26 ± 0.64^{b}	20.14 ± 0.80^{de}
P. aeruginosa	20.83 ± 0.28^{d}	17.20 ± 0.80^{fg}
Fungi		
C. albicans	30.20 ± 0.72^{a}	18.43 ± 0.51^{ef}
A. flavus	30.60 ± 0.52^{a}	28.33 ± 0.61^{b}

Table 1. Presents inhibition zone diameter (IZD) of *BCM*-AgNPs against selected pathogenic microorganisms. Positive control: ciprofloxacin and nystatin for bacteria and fungi, respectively. mm millimeter, SD (±) standard deviation, $n = 3$, mean values in the same column and across the rows that don't share the same superscript are significantly different ($P < 0.05$). However, those that share the same superscript are not significantly different ($P > 0.05$); One-way ANOVA (Tukey's test at 5% level).

AgNPs, with IZD values of 16.23, 17.20, and 18.43 mm, respectively. These results could be explained by the physiological and biological differences among microorganisms, such as differences in the composition of cell walls, distinct metabolic pathways between fungi and bacteria, as well as microorganism surface charge affecting nanoparticle interactions, which would influence the susceptibility of each microorganism to *BCM*-AgNPs compared to others[125]. Moreover, other studies have reported IZD higher than those found in our study. Amr et al.[67] have reported the IZD for biosynthesized AgNPs of 25, 28, and 48 mm against *E. coli*, *S. aureus*, and *P. aeruginosa*, respectively. These discrepancies may be attributed to variations in the bacterial strains, culture media, experimental conditions, and methodologies used[63,126].

Microorganism	MIC (µg/mL) of AgNPs							
	1000	500	250	125	62.5	31.25	15.62	7.81
S. aureus	-	-	-	+	+	+	+	+
E. coli	-	-	-	-	+	+	+	+
K. pneumoniae	-	-	-	+	+	+	+	+
P. aeruginosa	-	-	-	-	-	+	+	+
C. albicans	-	-	-	+	+	+	+	+
A. flavus	-	-	-	-	+	+	+	+
Spectrum activity (%)	6/6	6/6	6/6	3/6	1/6	0/6	0/6	0/6
	100	100	100	50	16.7	0	0	0

Table 2. Shows the MIC of *BCM*-AgNPs against selected pathogenic microorganisms. (-) no growth, (+) growth.

Microorganism	MBC (µg/mL) of AgNPs							
	1000	500	250	125	62.5	31.25	15.62	7.81
S. aureus	-	-	-	+	+	+	+	+
E. coli	-	-	-	+	+	+	+	+
K. pneumoniae	-	-	+	+	+	+	+	+
P. aeruginosa	-	-	-	-	+	+	+	+
C. albicans	-	-	+	+	+	+	+	+
A. flavus	-	-	-	-	+	+	+	+
Spectrum activity (%)	6/6	6/6	4/6	2/6	0/6	0/6	0/6	0/6
	100	100	66.67	33.33	0	0	0	0

Table 3. Shows the MBC of *BCM*-AgNPs against selected pathogenic microorganisms. (-) no growth, (+) growth.

Microorganism	MIC (µg/mL)	MBC or MFC (µg/mL)	MBC/MIC MFC/MIC	Mode of action
S. aureus	250	250	1	Bactericidal
E. coli	125	250	2	Bactericidal
K. pneumoniae	250	500	2	Bactericidal
P. aeruginosa	62.5	125	2	Bactericidal
C. albicans	250	500	2	Fungicidal
A. flavus	125	125	1	Fungicidal

Table 4. Shows the MIC, MBC, MFC, and mode of action of *BCM*-AgNPs. MIC: minimum inhibition concentration, MBC: minimum bactericidal concentration, MFC: minimum fungicidal concentration, Bactericidal effect: MBC/MIC or MFC/MIC ≤ 4.

The MIC and the MBC results of *BCM*-AgNPs on the tested pathogens are presented in Tables 2 and 3, respectively. *BCM*-AgNPs exhibited a lower MIC (lowest concentration of AgNPs at which no colony growth was observed) against *P. aeruginosa* (62.5 µg/mL), a two-fold higher MIC against *E. coli* and *A. flavus* (125 µg/mL), and a three-fold higher MIC against *S. aureus* and *C. albicans* (250 µg/mL). The findings demonstrated that *BCM*-AgNPs exhibited bactericidal and fungicidal effects against the tested bacteria and fungi at the respective MIC (Table 4), thereby validating their reported antimicrobial efficacy[67,125,127]. The MBC was found to be consistent across various bacterial and fungal species, measuring 125 µg/mL for *P. aeruginosa* and *A. flavus*, 250 µg/mL for *E. coli* and *S. aureus*, and 500 µg/mL for *K. pneumoniae* and *C. albicans*. The plate images corroborate all the MIC results, which indicate the absence of microbial growth at the MIC values, as shown in (Supplementary Figs. S1, S2, and S3).

P. aeruginosa has shown the highest sensitivity to *BCM*-AgNPs, with MIC and MBC values of 62.5 µg/mL and 125 µg/mL, respectively, compared to the other pathogens tested. Our findings align with external studies in this regard[125,128]. Studies have reported that the higher sensitivity exhibited by *P. aeruginosa* towards AgNPS could be attributed to the structure of the bacterial cell wall in gram-negative bacteria, which has a thinner peptidoglycan layer compared to gram-positive bacteria, making it easier for AgNPs to penetrate[20,129]. Moreover, the excellent efficacy of *BCM*-AgNPs against all tested microbial strains in this study could most likely be explained by the

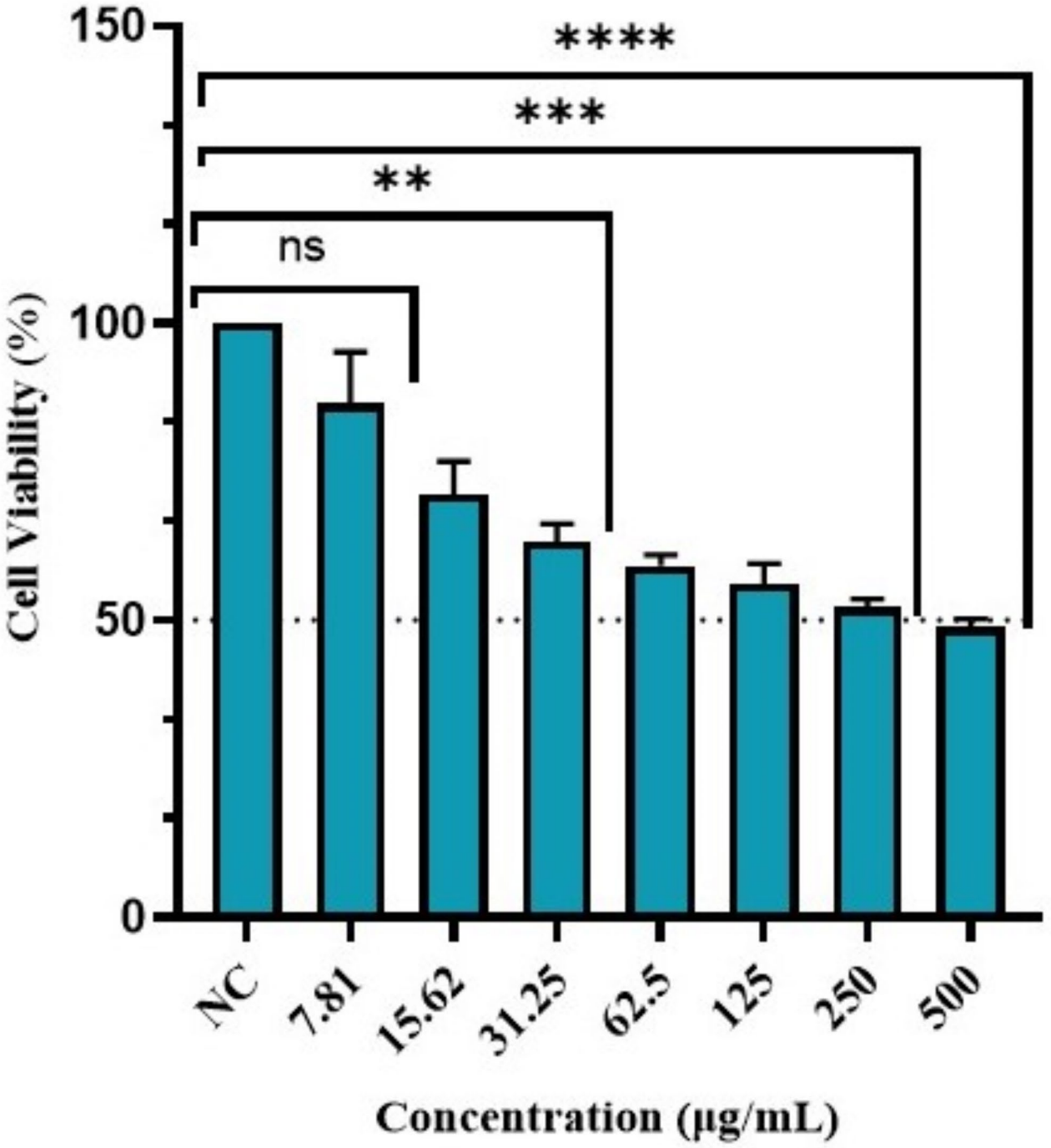

Fig. 14. Effect of *BCM*-AgNPs on Vero normal cell line viability. NC: negative control, $^{ns}p > 0.05$, $^{**}p < 0.001$, $^{***}p < 0.0001$ and $^{****}p < 0.0000$.

silver ion released by the AgNPs, which would damage the cell walls[130,131]. Furthermore, the antimicrobial properties of secondary metabolites adsorbed on the AgNPs have been reported by numerous studies[4].

The antimicrobial properties of *BCM*-AgNPs stem from various mechanisms of action that encompass diverse ways in which they inhibit or kill microorganisms. One of the mechanisms of action of *BCM*-AgNPs could be attributed to the overall positive charge of AgNPs, which plays a crucial role in their interaction with the negatively charged bacterial cell wall. This interaction leads to the alterations in the morphology of the cell wall and an increase in cell permeability, resulting in the leakage of cellular contents and, ultimately, cell death[67]. The presence of *BCM*-AgNPs reduces the transport of nutrients through the membrane, which relies entirely on its permeability. Furthermore, it inactivates proteins, ultimately leading to the death of bacterial cells[132]. In some cases, AgNPs disrupt bacterial enzymatic activities, affecting all metabolic processes (cell division, respiration,

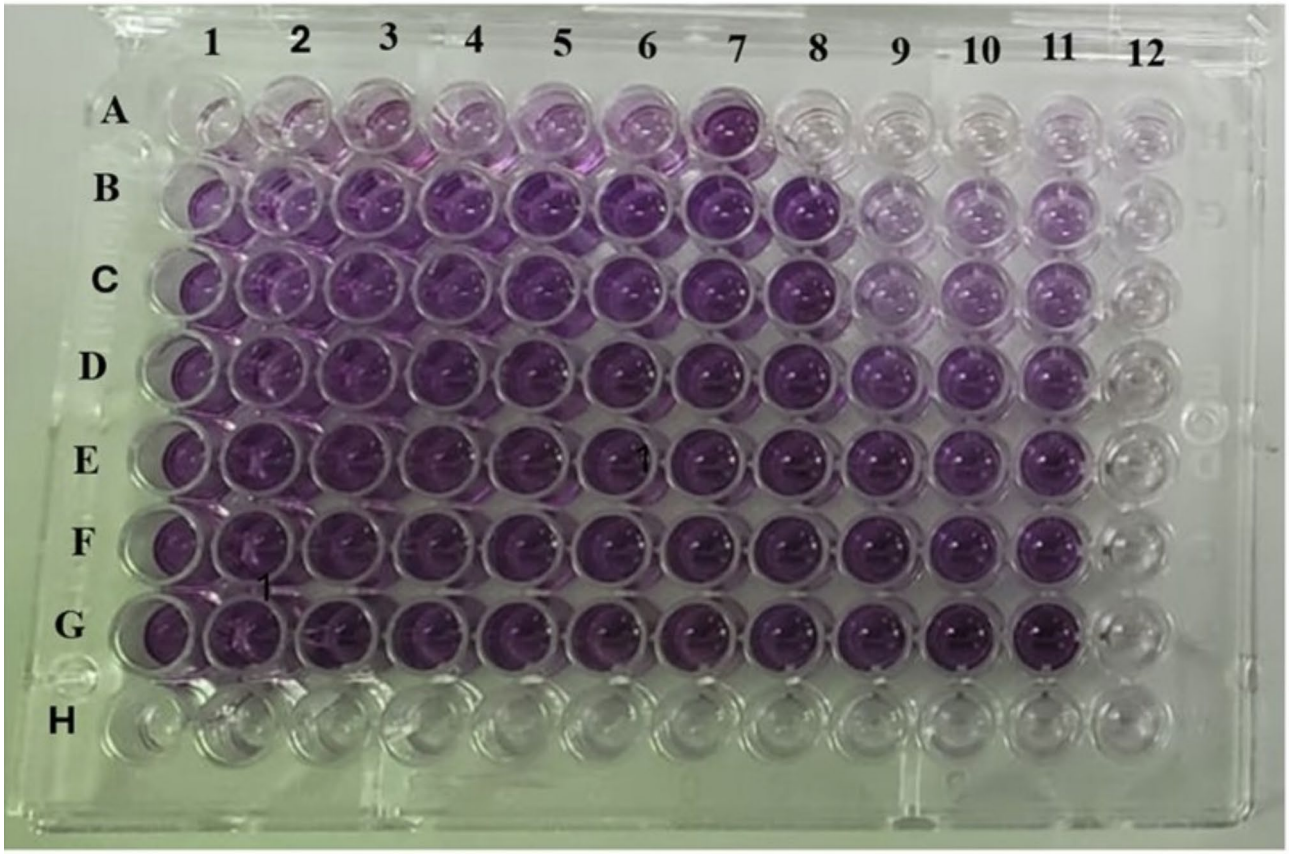

Fig. 15. Plate showing the MTT assay on Vero normal cell line.

survival of the cell)[131,133]. Moreover, studies have reported that AgNPs exhibit antimicrobial activity due to the presence of silver ions, which interfere with the electron transport chain in microorganisms or damage nucleic acids by binding to these biomolecules, leading to the death of the bacteria[4]. However, alternative studies have indicated that silver ions, when binding with nitrogen and sulphur, can inhibit and disrupt protein structures by attaching to thiol and amino groups. This process is notable because thiol groups are recognized for their role in triggering reactive oxygen species (ROS) production, which ultimately leads to the inhibition of respiratory enzymes and, afterward, the death of bacteria. On the other hand, *BCM*-AgNPs could release silver ions that hinder bacterial DNA replication by interacting with protein sulfhydryl groups[4].

Several studies have revealed that AgNPs produced from plants have strong anti-fungal activities against various types of fungi[67]. *BCM*-AgNPs effectively damage the fungal cell wall and destroy surface proteins and nucleic acids[134,135]. In addition, AgNPs can accumulate reactive oxygen species in fungal cells and impede proton pumps[134,135]. On the other hand, AgNPs assist in the buildup of silver ions, which induce respiratory blockage and subsequent damage to the electron transport system, ultimately leading to apoptosis[136]. Finally, AgNPs disrupt DNA replication and can interact with substrates through competitive inhibition, deactivating enzymes, and preventing the production of essential cellular products[135].

The safety of *BCM*-AgNPs was assessed in vitro using an MTT cytotoxicity assay on the Vero cell line, as depicted in Fig. 15. The results of Vero cells treated with *BCM*-AgNPs at different concentrations (7.81 µg/mL to 500 µg/mL) after 24 h of incubation are shown in Fig. 14. Assessing the cytotoxicity of any product intended for human use is vital to ensure product safety[137,138]. The findings indicate that the cells' viability decreased as the concentration of AgNPs increased[67,139]. Our results align with previous studies, which reported that high concentrations of AgNPs could increase cell membrane damage, thereby increasing mitochondrial membrane permeability and exposure to silver ions[140,141]. The cell viability in this study was recorded as 92. 66%, 62.12%, and 48.86%, with toxicity percentages of 7.33%, 39.88%, and 51.14% at 7.81 µg/mL, 62.5 µg/mL, and 500 µg/mL of AgNPs concentration, respectively. On the other hand, the IC50 was found to be 152.4 µg/mL, implying that the AgNPs did not show substantial cytotoxicity at the tested concentrations. Our findings align with previous studies that also reported an IC50 of 155 µg/mL for biosynthesized AgNPs[67]. Further study has reported that substances are generally categorized as non-cytotoxic if the IC50 value is equal to or greater than 90 µg/mL[142]. Thus, the biosynthesized *BCM*-AgNPs in this study are safe for use. The study's findings indicate that *BCM*-AgNPs exhibited good biocompatibility, making them suitable for various applications, including antimicrobial and anticancer agents. The novelty of this study lies in the use for the first time BCME for the green synthesis of AgNPs, offering an eco-friendly and sustainable method. By combining green chemistry with advanced antimicrobial applications, the study introduces a new approach to synthesizing biocompatible and effective

AgNPs, potentially addressing challenges such as antibiotic resistance and drug side effects through green nanobiotechnology.

Conclusions

Green synthesis of nanoparticles has emerged as a vital branch of nanotechnology due to its numerous benefits in diverse fields. This eco-friendly approach relies on the unique properties of secondary metabolites present in plants, which act as both reducing and stabilizing agents during the green synthesis of metallic nanoparticles. In this study, we employed the secondary metabolite in BCME to synthesize stable, spherical, and crystalline AgNPs. These *BCM*-AgNPs exhibited remarkable antimicrobial properties against both Gram-positive and Gram-negative bacteria, as well as antifungal properties. Moreover, the synthesized *BCM*-AgNPs exhibited minimal cytotoxicity against the normal Vero cell line, making them safe and biocompatible. The key findings of this study suggest that eco-friendly synthesized *BCM*-AgNPs appear as a promising alternative to tackle the emergence of multidrug-resistant strains. This study presents a novel approach to synthesizing AgNPs using a nutraceutical microgreen, offering a biocompatible and promising alternative for combating multi-drug resistance. Further investigations should focus on assessing the effectiveness of *BCM*-AgNPs against a wider array of pathogens, including viruses and more resistant strains. Furthermore, research should explore the underlying mechanisms of their antimicrobial and antifungal actions to refine their synthesis and improve their efficacy.

Data availability

The datasets generated and/or analyzed during the current study are available from the corresponding author on reasonable request.

Received: 26 June 2024; Accepted: 19 November 2024
Published online: 26 November 2024

References

1. Bayda, S., Adeel, M., Tuccinardi, T., Cordani, M. & Rizzolio, F. The history of nanoscience and nanotechnology: From chemical-physical applications to nanomedicine. *Molecules* **25**(1), 112. https://doi.org/10.3390/molecules25010112 (2019).
2. Rafique, M., Tahir, M. B., Rafique, M. S. & Hamza, M. History and fundamentals of nanoscience and nanotechnology. In *Nanotechnology and Photocatalysis for Environmental Applications. Micro and Nano Technologies* (eds Tahir, M. B. et al.) 1–25 (Elsevier, 2020).
3. Nagaraja, S. K., Niazi, S. K., Bepari, A., Assiri, R. A. & Nayaka, S. Leonotis nepetifolia flower bud extract mediated green synthesis of silver nanoparticles, their characterization, and in vitro evaluation of biological applications. *Materials* **15**, 24. https://doi.org/10.3390/ma15248990 (2022).
4. Asif, M. et al. Green synthesis of silver nanoparticles (AgNPs), structural characterization, and their antibacterial potential. *Dose Response* **20**(2), 15593258221088708. https://doi.org/10.1177/15593258221088709 (2022).
5. Mauricio, M. D. et al. Nanoparticles in medicine: A focus on vascular oxidative stress. *Oxid. Med. Cell Longev.* **2018**, 6231482. https://doi.org/10.1155/2018/6231482 (2018).
6. Yaraki, M. T. et al. Biomimetic metallic nanostructures for biomedical applications, catalysis, and beyond. *Ind. Eng. Chem. Res.* **61**(22), 7547–7593. https://doi.org/10.1021/acs.iecr.2c00285 (2022).
7. Khursheed, R. et al. Biomedical applications of metallic nanoparticles in cancer: Current status and future perspectives. *Biomed. Pharmacother.* **150**, 112951. https://doi.org/10.1016/j.biopha.2022.112951 (2022).
8. Kaabipour, S. & Hemmati, S. A review on the green and sustainable synthesis of silver nanoparticles and one-dimensional silver nanostructures. *Beilstein J. Nanotechnol.* **12**(1), 102–136. https://doi.org/10.3762/bjnano.12.9 (2021).
9. Dawadi, S. et al. Current research on silver nanoparticles: Synthesis, characterization, and applications. *J. Nanomater.* **2021**(1), 6687290. https://doi.org/10.1155/2021/6687290 (2021).
10. Parveen, K., Banse, V. & Ledwani, L. Green synthesis of nanoparticles: Their advantages and disadvantages. In *AIP Conference Proceedings* Vol. 1724 020048. https://doi.org/10.1063/1.4945168 (2016).
11. Kulkarni, D. et al. Biofabrication of nanoparticles: Sources, synthesis, and biomedical applications. *Front. Bioeng. Biotechnol.* https://doi.org/10.3389/fbioe.2023.1159193 (2023).
12. Rani, M., Yadav, J., Chaudhary, S. & Shanker, U. An updated review on synthetic approaches of green nanomaterials and their application for removal of water pollutants: Current challenges, assessment and future perspectives. *J. Environ. Chem. Eng.* **9**, 106763. https://doi.org/10.1016/j.jece.2021.106763 (2021).
13. Govindarajan, M. et al. Green synthesis and characterization of silver nanoparticles fabricated using *Anisomeles indica:* Mosquitocidal potential against malaria, dengue and Japanese encephalitis vectors. *Exp. Parasitol.* **161**, 40–47. https://doi.org/10.1016/j.exppara.2015.12.011 (2016).
14. Shashiraj, K. N. et al. Exploring the antimicrobial, anticancer, and apoptosis inducing ability of biofabricated silver nanoparticles using Lagerstroemia speciosa flower buds against the human osteosarcoma (MG-63) cell line via flow cytometry. *Bioengineering* **10**, 7. https://doi.org/10.3390/bioengineering10070821 (2023).
15. Chung, I.-M., Park, I., Seung-Hyun, K., Thiruvengadam, M. & Rajakumar, G. Plant-mediated synthesis of silver nanoparticles: Their characteristic properties and therapeutic applications. *Nanoscale Res. Lett.* **11**(1), 40. https://doi.org/10.1186/s11671-016-1257-4 (2016).
16. Muthukumaran, U., Govindarajan, M., Rajeswary, M. & Hoti, S. L. Synthesis and characterization of silver nanoparticles using Gmelina asiatica leaf extract against filariasis, dengue, and malaria vector mosquitoes. *Parasitol. Res.* **114**(5), 1817–1827. https://doi.org/10.1007/s00436-015-4368-4 (2015).
17. Maciel, M. V. et al. Green synthesis, characteristics and antimicrobial activity of silver nanoparticles mediated by essential oils as reducing agents. *Biocatal. Agric. Biotechnol.* **28**, 101746. https://doi.org/10.1016/j.bcab.2020.101746 (2020).
18. Alabdallah, N. M. & Hasan, Md. M. Plant-based green synthesis of silver nanoparticles and its effective role in abiotic stress tolerance in crop plants. *Saudi J. Biol. Sci.* **28**(10), 5631–5639. https://doi.org/10.1016/j.sjbs.2021.05.081 (2021).
19. Ahmed, A. et al. Nature-inspired biogenic synthesis of silver nanoparticles for antibacterial applications. *Mater. Today Chem.* **27**, 101339. https://doi.org/10.1016/j.mtchem.2022.101339 (2023).
20. Menichetti, A., Mavridi-Printezi, A., Mordini, D. & Montalti, M. Effect of size, shape and surface functionalization on the antibacterial activity of silver nanoparticles. *J. Funct. Biomater.* **14**, 5. https://doi.org/10.3390/jfb14050244 (2023).
21. Restrepo, C. V. & Villa, C. C. Synthesis of silver nanoparticles, influence of capping agents, and dependence on size and shape: A review. *Environ. Nanotechnol. Monit. Manag.* **15**, 100428. https://doi.org/10.1016/j.enmm.2021.100428 (2021).

22. Dakal, T. C., Kumar, A., Majumdar, R. S. & Yadav, V. Mechanistic basis of antimicrobial actions of silver nanoparticles. *Front. Microbiol.* https://doi.org/10.3389/fmicb.2016.01831 (2016).
23. Stabryla, L. M., Moncure, P. J., Millstone, J. E. & Gilbertson, L. M. Particle-driven effects at the bacteria interface: A nanosilver investigation of particle shape and dose metric. *ACS Appl. Mater. Interfaces* **15**(33), 39027–39038. https://doi.org/10.1021/acsami.3c00144 (2023).
24. Nayaka, S. et al. Biosynthesis, characterization, and in vitro assessment on cytotoxicity of actinomycete-synthesized silver nanoparticles on Allium cepa root tip cells. *Beni Suef Univ. J. Basic Appl. Sci.* **9**(1), 51. https://doi.org/10.1186/s43088-020-00074-8 (2020).
25. Tanwar, M., Meena, J. & Meena, L. S. Nanoparticles: Scope in drug delivery. In *Advanced Biomaterials and Biodevices* 487–521 (John Wiley & Sons Ltd, 2014).
26. Alara, J. A. & Alara, O. R. An Overview of the global alarming increase of multiple drug resistant: A major challenge in clinical diagnosis. *Infect. Disord. Drug TargetsDisorders* **24**, 26–42. https://doi.org/10.2174/1871526523666230725103902 (2024).
27. Salam, M. A. et al. Antimicrobial resistance: A growing serious threat for global public health. *Healthcare* **11**, 13. https://doi.org/10.3390/healthcare11131946 (2023).
28. Bar, H. et al. Green synthesis of silver nanoparticles using latex of *Jatropha curcas*. *Colloids Surf. A Physicochem. Eng. Asp.* **339**, 134–139. https://doi.org/10.1016/j.colsurfa.2009.02.008 (2009).
29. Altun, E. et al. Metal-based nanoparticles for combating antibiotic resistance. *Appl. Phys. Rev.* **8**(4), 041303. https://doi.org/10.1063/5.0060299 (2021).
30. Zou, W., McAdorey, A., Yan, H. & Chen, W. Nanomedicine to overcome antimicrobial resistance: Challenges and prospects. *Nanomedicine* **18**(5), 471–484. https://doi.org/10.2217/nnm-2023-0022 (2023).
31. Nagaraja, S. K. et al. Biomimetic synthesis of silver nanoparticles using Cucumis sativus var. hardwickii fruit extract and their characterizations, anticancer potential and apoptosis studies against Pa-1 (Human ovarian teratocarcinoma) cell line via flow cytometry. *Appl. Nanosci.* **13**(4), 3073–3084. https://doi.org/10.1007/s13204-022-02386-w (2023).
32. Velusamy, P., Das, J., Pachaiappan, R., Vaseeharan, B. & Pandian, K. Greener approach for synthesis of antibacterial silver nanoparticles using aqueous solution of neem gum (Azadirachta indica L.). *Ind. Crops Prod.* **66**, 103–109. https://doi.org/10.1016/j.indcrop.2014.12.042 (2015).
33. Golli, R. et al. Silver nanoparticles synthesized by Brassica oleracea (Broccoli) acting as antifungal agent against Candida albicans. *Mater. Today Proc.* **80**, 1495–1500. https://doi.org/10.1016/j.matpr.2023.01.284 (2023).
34. Bhat, M. P. et al. Characterization, antimicrobial activity and anticancer activity of Pyrostegia venusta leaf extract-synthesized silver nanoparticles against COS-7 cell line. *Appl. Nanosci.* **13**(3), 2303–2314. https://doi.org/10.1007/s13204-021-02120-y (2022).
35. Pant, Y., Lingwan, M. & Masakapalli, S. K. Metabolic, biochemical, mineral and fatty acid profiles of edible *Brassicaceae* microgreens establish them as promising functional food. *Food Chem. Adv.* **3**, 100461. https://doi.org/10.1016/j.focha.2023.100461 (2023).
36. Maru, R. et al. Evaluation of growth, yield and bioactive compounds of Ethiopian Kale (Brassica carinata A. Braun) microgreens under different LED Light spectra and substrates. *Horticulturae* **10**, 436. https://doi.org/10.3390/horticulturae10050436 (2024).
37. Zhang, S., Mo, Z., Zhang, S. & Li, X. A network pharmacology approach to reveal the underlying mechanisms of artemisia annua on the treatment of Hepatocellular carcinoma. *Evid. Based Complement. Altern. Med.* **2021**, 8947304. https://doi.org/10.1155/2021/8947304 (2021).
38. Nakakaawa, L., Gbala, I. D., Cheseto, X., Bargul, J. L. & Wesonga, J. M. Oral acute, sub-acute toxicity and phytochemical profile of *Brassica carinata* A. Braun microgreens ethanolic extract in Wistar rats. *J. Ethnopharmacol.* **305**, 116121. https://doi.org/10.1016/j.jep.2022.116121 (2023).
39. Hagos, R. et al. Ethiopian mustard (Brassica carinata A. Braun) as an alternative energy source and sustainable crop. *Sustainability* **12**, 18. https://doi.org/10.3390/su12187492 (2020).
40. El-Nakhel, C. et al. Nutrient supplementation configures the bioactive profile and production characteristics of three *Brassica L.* microgreens species grown in peat-based media. *Agronomy* **11**, 346. https://doi.org/10.3390/agronomy11020346 (2021).
41. Martínez-Ispizua, E. et al. The nutritional quality potential of microgreens, baby leaves, and adult lettuce: An underexploited nutraceutical source. *Foods* **11**(3), 423. https://doi.org/10.3390/foods11030423 (2022).
42. Odongo, G. A. et al. The role of plant processing for the cancer preventive potential of Ethiopian kale (Brassica carinata). *Food Nutr. Res.* https://doi.org/10.1080/16546628.2017.1271527 (2017).
43. Gunasekaran, T., Haile, T., Nigusse, T. & Dhanaraju, M. D. Nanotechnology: An effective tool for enhancing bioavailability and bioactivity of phytomedicine. *Asian Pac. J. Trop. Biomed.* **4**, S1–S7. https://doi.org/10.12980/APJTB.4.2014C980 (2014).
44. Gavamukulya, Y. et al. Green synthesis and characterization of highly stable silver nanoparticles from ethanolic extracts of fruits of Annona muricata. *J. Inorg. Organomet. Polym.* **30**(4), 1231–1242. https://doi.org/10.1007/s10904-019-01262-5 (2020).
45. Son Phan, K. et al. Allium sativum @AgNPs and Phyllanthus urinaria @AgNPs: A comparative analysis for antibacterial application. *RSC Adv.* **12**, 35730–35743. https://doi.org/10.1039/D2RA06847H (2022).
46. Bonifácio, B. V. et al. Nanotechnology-based drug delivery systems and herbal medicines: A review. *Int. J. Nanomed.* **9**, 1–15. https://doi.org/10.2147/IJN.S52634 (2014).
47. Mohammed, A. E. et al. In silico prediction of Malvaviscus arboreus metabolites and green synthesis of silver nanoparticles—opportunities for safer anti-bacterial and anti-cancer precision medicine. *Int. J. Nanomed.* **18**, 2141–2162. https://doi.org/10.2147/IJN.S400195 (2023).
48. Murugesan, K., Mulugeta, K., Hailu, E., Tamene, W. & Alagar Yadav, S. Insights for integrative medicinal potentials of Ethiopian Kale (Brassica carinata): Investigation of antibacterial, antioxidant potential and phytocompounds composition of its leaves. *Chin. Herb. Med.* **13**, 250–254. https://doi.org/10.1016/j.chmed.2020.09.003 (2020).
49. Khan, R., Mohamad Ghazali, F., Mahyudin, N. A. & Samsudin, N. I. P. Morphological characterization and determination of aflatoxigenic and non-aflatoxigenic aspergillus flavus isolated from sweet corn kernels and soil in Malaysia. *Agriculture* https://doi.org/10.3390/agriculture10100450 (2020).
50. Anandalakshmi, K., Venugobal, J. & Ramasamy, V. Characterization of silver nanoparticles by green synthesis method using Pedalium murex leaf extract and their antibacterial activity. *Appl. Nanosci.* **6**(3), 399–408. https://doi.org/10.1007/s13204-015-0449-z (2016).
51. Nzilu, D. M. et al. Green synthesis of copper oxide nanoparticles and its efficiency in degradation of rifampicin antibiotic. *Sci. Rep.* **13**(1), 14030. https://doi.org/10.1038/s41598-023-41119-z (2023).
52. Mpelane, S., Mketo, N., Bingwa, N. & Nomngongo, P. N. Synthesis of mesoporous iron oxide nanoparticles for adsorptive removal of levofloxacin from aqueous solutions: Kinetics, isotherms, thermodynamics and mechanism. *Alex. Eng. J.* **61**(11), 8457–8468. https://doi.org/10.1016/j.aej.2022.02.014 (2022).
53. El-Far, A. et al. Nanonutraceuticals: Anti-cancer activity and improved safety of chemotherapy by costunolide and its nanoformulation against colon and breast cancer. *Biomedicines* **9**(8), 990. https://doi.org/10.3390/biomedicines9080990 (2021).
54. Wanjiru, J., Gathirwa, J., Sauli, E. & Swai, H. S. Formulation, optimization, and evaluation of moringa oleifera leaf polyphenol-loaded phytosome delivery system against breast cancer cell lines. *Molecules* **27**(14), 4430. https://doi.org/10.3390/molecules27144430 (2022).
55. Kumar, R., Ghoshal, G. & Goyal, M. Rapid green synthesis of silver nanoparticles (AgNPs) using (Prunus persica) plants extract: Exploring its antimicrobial and catalytic activities. *J. Nanomed. Nanotechnol.* **8**, 452 (2017).

56. Hoang, V. T. et al. Functionalized-AgNPs for long-term stability and its applicability in the detection of manganese ions. *Adv. Polym. Technol.* https://doi.org/10.1155/2020/9437108 (2020).
57. Mwangi, W. C., Waudo, W., Shigwenya, M. E. & Gichuki, J. Phytochemical characterization, antimicrobial and antioxidant activities of Terminalia catappa methanol and aqueous extracts. *BMC Complement. Med. Ther.* **24**, 137. https://doi.org/10.1186/s12906-024-04449-7 (2024).
58. Odongo, E. A. et al. Evaluation of the antibacterial activity of selected Kenyan medicinal plant extract combinations against clinically important bacteria. *BMC Complement. Med. Ther.* **23**(1), 100. https://doi.org/10.1186/s12906-023-03939-4 (2023).
59. Madivoli, E. S. et al. Facile synthesis of silver nanoparticles using lantana trifolia aqueous extracts and their antibacterial activity. *J. Inorg. Organomet. Polym.* **30**(8), 2842–2850. https://doi.org/10.1007/s10904-019-01432-5 (2020).
60. Sengera, G. O., Kenanda, E. O. & Onyancha, J. M. Antibacterial, antioxidant potency, and chemical composition of essential oils from dried powdered leaves and flowers of Hypericum revolutum subsp. keniense (Schweinf.). *Evid. Based Complement. Altern. Med.* **2023**, 4125885. https://doi.org/10.1155/2023/4125885 (2023).
61. Hassan, A. & Ullah, H. Antibacterial and antifungal activities of the medicinal plant *Veronica biloba*. *J. Chem.* **2019**, e5264943. https://doi.org/10.1155/2019/5264943 (2019).
62. Humphries, R. M. et al. CLSI methods development and standardization working group best practices for evaluation of antimicrobial susceptibility tests. *J. Clin. Microbiol.* https://doi.org/10.1128/jcm.01934-17 (2018).
63. Xin, J. et al. Antibacterial activity and mechanism of chelerythrine against Streptococcus agalactiae. *Front. Vet. Sci.* https://doi.org/10.3389/fvets.2024.1408376 (2024).
64. CLSI. CLSI - M07-A10 - Methods for Dilution Antimicrobial Susceptibility Tests for Bacteria That Grow Aerobically; Approved Standard | GlobalSpec. Accessed 01 Oct 2024. Available: https://standards.globalspec.com/std/1537900/M07-A10.
65. Elshikh, M. et al. Resazurin-based 96-well plate microdilution method for the determination of minimum inhibitory concentration of biosurfactants. *Biotechnol. Lett.* **38**(6), 1015–1019. https://doi.org/10.1007/s10529-016-2079-2 (2016).
66. Teh, C. H., Nazni, W. A., Nurulhusna, A. H., Norazah, A. & Lee, H. L. Determination of antibacterial activity and minimum inhibitory concentration of larval extract of fly via resazurin-based turbidometric assay. *BMC Microbiol.* **17**(1), 36. https://doi.org/10.1186/s12866-017-0936-3 (2017).
67. Amr, M. et al. Utilization of biosynthesized silver nanoparticles from Agaricus bisporus extract for food safety application: synthesis, characterization, antimicrobial efficacy, and toxicological assessment. *Sci. Rep.* **13**(1), 15048. https://doi.org/10.1038/s41598-023-42103-3 (2023).
68. Parvekar, P., Palaskar, J., Metgud, S., Maria, R. & Dutta, S. The minimum inhibitory concentration (MIC) and minimum bactericidal concentration (MBC) of silver nanoparticles against Staphylococcus aureus. *Biomater. Investig. Dent.* **7**(1), 105–109. https://doi.org/10.1080/26415275.2020.1796674 (2020).
69. Mosmann, T. Rapid colorimetric assay for cellular growth and survival: Application to proliferation and cytotoxicity assays. *J. Immunol. Methods* **65**(1–2), 55–63. https://doi.org/10.1016/0022-1759(83)90303-4 (1983).
70. Ndacyayisenga, J., Maina, E. N., Ngeny, L. C., Wamunyokoli, F. & Tolo, F. M. Purple tea catechins exhibit high antiproliferative activity and synergism with cisplatin against the triple-negative breast cancer cell line 4T1. *Arch. Biol. Sci.* **75**, 4. https://doi.org/10.2298/ABS230816039N (2023).
71. Pauzi, A. Z. M. et al. Combination of cisplatin and bromelain exerts synergistic cytotoxic effects against breast cancer cell line MDA-MB-231 in vitro. *Chin. Med.* **11**, 46. https://doi.org/10.1186/s13020-016-0118-5 (2016).
72. Ghojavand, S., Madani, M. & Karimi, J. Green synthesis, characterization and antifungal activity of silver nanoparticles using stems and flowers of felty germander. *J. Inorg. Organomet. Polym.* **30**(8), 2987–2997. https://doi.org/10.1007/s10904-020-01449-1 (2020).
73. Sharma, K., Guleria, S. & Razdan, V. K. Green synthesis of silver nanoparticles using Ocimum gratissimum leaf extract: Characterization, antimicrobial activity and toxicity analysis. *J. Plant Biochem. Biotechnol.* **29**(2), 213–224. https://doi.org/10.1007/s13562-019-00522-2 (2020).
74. Goldstein, M. *Infrared Characteristic Group Frequencies* (Wiley, 1980).
75. Ghasemi, S. et al. Process optimization for green synthesis of silver nanoparticles using Rubus discolor leaves extract and its biological activities against multi-drug resistant bacteria and cancer cells. *Sci. Rep.* **14**(1), 4130. https://doi.org/10.1038/s41598-024-54702-9 (2024).
76. Kebede, T., Gadisa, E. & Tufa, A. Antimicrobial activities evaluation and phytochemical screening of some selected medicinal plants: A possible alternative in the treatment of multidrug-resistant microbes. *PLOS ONE* **16**(3), e0249253. https://doi.org/10.1371/journal.pone.0249253 (2021).
77. Wahab, S. et al. Metallic nanoparticles: A promising arsenal against antimicrobial resistance—unraveling mechanisms and enhancing medication efficacy. *Int. J. Mol. Sci.* **24**, 19. https://doi.org/10.3390/ijms241914897 (2023).
78. Jaffar, S. S. et al. Green synthesis of flower-like carrageenan-silver nanoparticles and elucidation of its physicochemical and antibacterial properties. *Molecules* **28**, 2. https://doi.org/10.3390/molecules28020907 (2023).
79. Smitha, S. L., Nissamudeen, K. M., Philip, D. & Gopchandran, K. G. Studies on surface plasmon resonance and photoluminescence of silver nanoparticles. *Spectrochim. Acta Part A Mol. Biomol. Spectrosc.* **71**(1), 186–190. https://doi.org/10.1016/j.saa.2007.12.002 (2008).
80. Zhang, X.-F., Liu, Z.-G., Shen, W. & Gurunathan, S. Silver nanoparticles: Synthesis, characterization, properties, applications, and therapeutic approaches. *Int. J. Mol. Sci.* **17**, 9 (2016).
81. Paul, T. K. et al. Mapping the progress in surface plasmon resonance analysis of phytogenic silver nanoparticles with colorimetric sensing applications. *Chem. Biodivers.* **20**(8), e202300510. https://doi.org/10.1002/cbdv.202300510 (2023).
82. Maitra, B. et al. Biosynthesis of *Bixa orellana* seed extract mediated silver nanoparticles with moderate antioxidant, antibacterial and antiproliferative activity. *Arab. J. Chem.* **16**(5), 104675. https://doi.org/10.1016/j.arabjc.2023.104675 (2023).
83. Akintelu, S. A. & Folorunso, A. Characterization and antimicrobial investigation of synthesized silver nanoparticles from Annona muricata leaf extracts. *Nanotechnol. Nanomed. Nanobiotechnol.* **6**, 1–4. https://doi.org/10.24966/NTMB-2044/100022 (2018).
84. Chinnasamy, R. et al. Eco-friendly synthesis of Ag-NPs using *Endostemon viscosus* (Lamiaceae): Antibacterial, antioxidant, larvicidal, photocatalytic dye degradation activity and toxicity in zebrafish embryos. *Environ. Res.* **218**, 114946. https://doi.org/10.1016/j.envres.2022.114946 (2023).
85. Mat Yusuf, S. N. A. et al. Optimization of biogenic synthesis of silver nanoparticles from flavonoid-rich *Clinacanthus nutans* leaf and stem aqueous extracts. *R. Soc. Open Sci.* **7**, 200065. https://doi.org/10.1098/rsos.200065 (2020).
86. Yousefbeyk, F. et al. Green synthesis of silver nanoparticles from *Stachys byzantina* K. Koch: Characterization, antioxidant, antibacterial, and cytotoxic activity. *Part. Sci. Technol.* **40**, 219–232. https://doi.org/10.1080/02726351.2021.1930302 (2022).
87. Asefian, S. & Ghavam, M. Green and environmentally friendly synthesis of silver nanoparticles with antibacterial properties from some medicinal plants. *BMC Biotechnol.* **24**(1), 5. https://doi.org/10.1186/s12896-023-00828-z (2024).
88. Yassin, M., Mostafa, A. A., Al-Askar, A. & Alotibi, F. Facile green synthesis of silver nanoparticles using aqueous leaf extract of origanum majorana with potential bioactivity against multidrug resistant bacterial strains. *Crystals* https://doi.org/10.3390/cryst12050603 (2022).
89. Shah, M., Fawcett, D., Sharma, S., Tripathy, S. K. & Poinern, G. E. J. Green Synthesis of metallic nanoparticles via biological entities. *Materials* **8**(11), 7278–7308. https://doi.org/10.3390/ma8115377 (2015).
90. Ahmed, S., Ahmad, M., Swami, B. L. & Ikram, S. A review on plants extract mediated synthesis of silver nanoparticles for antimicrobial applications: A green expertise. *J. Adv. Res.* **7**(1), 17–28. https://doi.org/10.1016/j.jare.2015.02.007 (2016).

91. Pham, N. B. T. et al. SERS behaviors of multi-shape silver nanoparticles on Si substrate—An insight from both experimental and theoretical approaches. *Colloids Surf. A Physicochem. Eng. Asp.* **684**, 133091. https://doi.org/10.1016/j.colsurfa.2023.133091 (2024).
92. Sudha, A., Jeyakanthan, J. & Srinivasan, P. Green synthesis of silver nanoparticles using *Lippia nodiflora* aerial extract and evaluation of their antioxidant, antibacterial and cytotoxic effects. *Resour. Effic. Technol.* **3**(4), 506–515. https://doi.org/10.1016/j.reffit.2017.07.002 (2017).
93. Nayak, P. S. et al. Silver nanoparticles fabricated using medicinal plant extracts show enhanced antimicrobial and selective cytotoxic propensities. *IET Nanobiotechnol.* **13**(2), 193–201. https://doi.org/10.1049/iet-nbt.2018.5025 (2019).
94. Samuggam, S. et al. Green synthesis and characterization of silver nanoparticles using spondias mombin extract and their antimicrobial activity against biofilm-producing bacteria. *Molecules* **26**, 9. https://doi.org/10.3390/molecules26092681 (2021).
95. Baran, A. et al. Investigation of antimicrobial and cytotoxic properties and specification of silver nanoparticles (AgNPs) derived from *Cicer arietinum* L. green leaf extract. *Front. Bioeng. Biotechnol.* https://doi.org/10.3389/fbioe.2022.855136 (2022).
96. Jyoti, K., Baunthiyal, M. & Singh, A. Characterization of silver nanoparticles synthesized using *Urtica dioica* Linn. leaves and their synergistic effects with antibiotics. *J. Radiat. Res. Appl. Sci.* **9**(3), 217–227. https://doi.org/10.1016/j.jrras.2015.10.002 (2016).
97. Soyucok, A., Kabak, B. & Tosun, B. Optimization of synthesis reaction parameters of AgNPs derived from *Laser trilobum* plant for foodborne pathogens. *Food Bioprocess. Technol.* https://doi.org/10.1007/s11947-024-03359-3 (2024).
98. Azizi, M., Sedaghat, S., Tahvildari, K., Derakhshi, P. & Ghaemi, A. Green biosynthesis of silver nanoparticles with *Eryngium caucasicum* Trautv aqueous extract. *Inorg. Nano Metal Chem.* **50**(6), 429–436. https://doi.org/10.1080/24701556.2020.1716010 (2020).
99. Mahiuddin, M., Saha, P. & Ochiai, B. Green synthesis and catalytic activity of silver nanoparticles based on piper chaba stem extracts. *Nanomaterials* **10**, 9. https://doi.org/10.3390/nano10091777 (2020).
100. Hanna, A. L. et al. Biosynthesis and characterization of silver nanoparticles produced by *Phormidium ambiguum* and *Desertifilum tharense* cyanobacteria. *Bioinorg. Chem. Appl.* **2022**(1), 9072508. https://doi.org/10.1155/2022/9072508 (2022).
101. Masum, M. M. I. et al. Biogenic synthesis of silver nanoparticles using phyllanthus emblica fruit extract and its inhibitory action against the pathogen *Acidovorax oryzae* strain RS-2 of rice bacterial brown stripe. *Front. Microbiol.* **10**. https://doi.org/10.3389/fmicb.2019.00820 (2019).
102. Naim, R. H. et al. Biosynthesis, antimicrobial and in vitro antiproliferative activities of silver/silver chloride nanoparticles from mixed fruit extracts of *Capsicum frutescens* and *Tamarindus indica*. *Food Chem. Adv.* **5**, 100773. https://doi.org/10.1016/j.focha.2024.100773 (2024).
103. Levard, C. et al. Effect of chloride on the dissolution rate of silver nanoparticles and toxicity to *E. coli*. *Environ. Sci. Technol.* **47**, 5738–5745. https://doi.org/10.1021/es400396f (2013).
104. De Barros, C. H. N., Cruz, G. C. F., Mayrink, W. & Tasic, L. Bio-based synthesis of silver nanoparticles from orange waste: Effects of distinct biomolecule coatings on size, morphology, and antimicrobial activity. *Nanotechnol. Sci. Appl.* **11**, 1–14. https://doi.org/10.2147/nsa.s156115 (2018).
105. Rautela, A., Rani, J. & Debnath, M. Green synthesis of silver nanoparticles from Tectona grandis seeds extract: Characterization and mechanism of antimicrobial action on different microorganisms. *J. Anal. Sci. Technol.* **10**, 5. https://doi.org/10.1186/s40543-018-0163-z (2019).
106. Tomaszewska, E. et al. Detection limits of DLS and UV-vis spectroscopy in characterization of polydisperse nanoparticles colloids. *J. Nanomater.* **2013**. https://doi.org/10.1155/2013/313081 (2013).
107. Jia, Z., Li, J., Gao, L., Yang, D. & Kanaev, A. Dynamic light scattering: A powerful tool for in situ nanoparticle sizing. *Colloids Interfaces* **7**, 1. https://doi.org/10.3390/colloids7010015 (2023).
108. Ezealisiji, K. M., Noundou, X. S. & Ukwueze, S. E. Green synthesis and characterization of monodispersed silver nanoparticles using root bark aqueous extract of *Annona muricata* Linn and their antimicrobial activity. *Appl. Nanosci.* **7**, 905–911. https://doi.org/10.1007/s13204-017-0632-5 (2017).
109. Danaei, M. et al. Impact of particle size and polydispersity index on the clinical applications of lipidic nanocarrier systems. *Pharmaceutics* **10**, 57. https://doi.org/10.3390/pharmaceutics10020057 (2018).
110. Subramaniam, B., Siddik, Z. H. & Nagoor, N. H. Optimization of nanostructured lipid carriers: Understanding the types, designs, and parameters in the process of formulations. *J. Nanopart. Res.* **22**, 141. https://doi.org/10.1007/s11051-020-04848-0 (2020).
111. Clarke, S. P. Development of Hierarchical Magnetic Nanocomposite Materials for Biomedical Applications. Accessed: May 05, 2024. Available: https://www.semanticscholar.org/paper/Development-of-Hierarchical-Magnetic-Nanocomposite-Clarke (2013).
112. Gatto, M. S. & Najahi-Missaoui, W. Lyophilization of nanoparticles, does it really work? Overview of the current status and challenges. *Int. J. Mol. Sci.* **24**, 18. https://doi.org/10.3390/ijms241814041 (2023).
113. Singh, S., Bharti, A. & Meena, V. K. Structural, thermal, zeta potential and electrical properties of disaccharide reduced silver nanoparticles. *J. Mater. Sci. Mater. Electron.* **25**, 3747–3752. https://doi.org/10.1007/s10854-014-2085-x (2014).
114. Xu, L. et al. Lipid nanoparticles for drug delivery. *Adv. NanoBiomed Res.* **2**, 2100109. https://doi.org/10.1002/anbr.202100109 (2022).
115. Giri, A. K. et al. Green synthesis and characterization of silver nanoparticles using Eugenia roxburghii DC. extract and activity against biofilm-producing bacteria. *Sci. Rep.* **12**, 8383. https://doi.org/10.1038/s41598-022-12484-y (2022).
116. Arshad, H., Sami, M. A., Sadaf, S. & Hassan, U. Salvadora persica mediated synthesis of silver nanoparticles and their antimicrobial efficacy. *Sci. Rep.* **11**, 5996. https://doi.org/10.1038/s41598-021-85584-w (2021).
117. Ahmad, K. et al. Green synthesis and characterization of silver nanoparticles through the Piper cubeba ethanolic extract and their enzyme inhibitory activities. *Front. Chem.* **11**. https://doi.org/10.3389/fchem.2023.1065986 (2023).
118. Liaqat, N., Jahan, N., Rahman, K. U., Anwar, T. & Qureshi, H. Green synthesized silver nanoparticles: Optimization, characterization, antimicrobial activity, and cytotoxicity study by hemolysis assay. *Front. Chem.* **10**, 952006. https://doi.org/10.3389/fchem.2022.952006 (2022).
119. Velgosová, O. & Mražíková, A. Green synthesis, long-term stability and toxicity of colloidal Ag nanoparticles. *Wseas Trans. Biol. Biomed.* **14** (2017).
120. Xin, X., Qi, C., Xu, L., Gao, Q. & Liu, X. Green synthesis of silver nanoparticles and their antibacterial effects. *Front. Chem. Eng.* **4**. https://doi.org/10.3389/fceng.2022.941240 (2022).
121. Arya, A. et al. Biosynthesis and assessment of antibacterial and antioxidant activities of silver nanoparticles utilizing *Cassia occidentalis* L. seed. *Sci Rep* **14**, 7243. https://doi.org/10.1038/s41598-024-57823-3 (2024).
122. Bolatchiev, A. Antibacterial activity of human defensins against *Staphylococcus aureus* and *Escherichia coli*. *PeerJ* **8**, e10455. https://doi.org/10.7717/peerj.10455 (2020).
123. Zhou, L. et al. Antifungal activity of silver nanoparticles synthesized by iturin against *Candida albicans* in vitro and in vivo. *Appl. Microbiol. Biotechnol.* **105**, 3759–3770. https://doi.org/10.1007/s00253-021-11296-w (2021).
124. Ma, X., Wang, Z., Liu, R. & Jiang, Y. Effect of powdery mildew on interleaf microbial communities and leaf antioxidant enzyme systems. *J. For. Res.* **34**, 1535–1547. https://doi.org/10.1007/s11676-023-01597-3 (2023).
125. Alqahtani, M. A., Al Othman, M. R. & Mohammed, A. E. Bio fabrication of silver nanoparticles with antibacterial and cytotoxic abilities using lichens. *Sci. Rep.* **10**(1), 16781. https://doi.org/10.1038/s41598-020-73683-z (2020).
126. He, Z., Huang, Z., Jiang, W. & Zhou, W. Antimicrobial activity of cinnamaldehyde on streptococcus mutans biofilms. *Front. Microbiol.* **10**. https://doi.org/10.3389/fmicb.2019.02241 (2019).

127. Rizwana, H. et al. Antimicrobial and antioxidant potential of the silver nanoparticles synthesized using aqueous extracts of coconut meat (*Cocos nucifera* L). *Sci. Rep.* **13**(1), 16270. https://doi.org/10.1038/s41598-023-43384-4 (2023).
128. Salayová, A. et al. Green synthesis of silver nanoparticles with antibacterial activity using various medicinal plant extracts: Morphology and antibacterial efficacy. *Nanomaterials* **11**(4), 1005. https://doi.org/10.3390/nano11041005 (2021).
129. Din, L. B. et al. Synthesis of silver nanoparticles with antibacterial activity using the lichen Parmotrema praesorediosum. *Int. J. Nanomed.* **9**, 121–127. https://doi.org/10.2147/IJN.S52306 (2014).
130. Elemike, E. E., Onwudiwe, D. C., Ekennia, A. C., Ehiri, R. C. & Nnaji, N. J. Phytosynthesis of silver nanoparticles using aqueous leaf extracts of *Lippia citriodora*: Antimicrobial, larvicidal and photocatalytic evaluations. *Mater. Sci. Eng. C* **75**, 980–989. https://doi.org/10.1016/j.msec.2017.02.161 (2017).
131. More, P. R. et al. Silver nanoparticles: Bactericidal and mechanistic approach against drug resistant pathogens. *Microorganisms* **11**, 2. https://doi.org/10.3390/microorganisms11020369 (2023).
132. Saqib, S. et al. Bimetallic assembled silver nanoparticles impregnated in *Aspergillus fumigatus* extract damage the bacterial membrane surface and release cellular contents. *Coatings* **12**, 10. https://doi.org/10.3390/coatings12101505 (2022).
133. Egger, S., Lehmann, R. P., Height, M. J., Loessner, M. J. & Schuppler, M. Antimicrobial properties of a novel silver-silica nanocomposite material. *Appl. Environ. Microbiol.* **75**(9), 2973–2976. https://doi.org/10.1128/AEM.01658-08 (2009).
134. Mansoor, S. et al. Fabrication of silver nanoparticles against fungal pathogens. *Front. Nanotechnol.* **3**. https://doi.org/10.3389/fnano.2021.679358 (2021).
135. Hashem, A. H. et al. Antifungal activity of biosynthesized silver nanoparticles (AgNPs) against Aspergilli causing Aspergillosis: Ultrastructure study. *J. Funct. Biomater.* **13**(4), 242. https://doi.org/10.3390/jfb13040242 (2022).
136. Du, H., Lo, T.-M., Sitompul, J. & Chang, M. W. Systems-level analysis of *Escherichia coli* response to silver nanoparticles: The roles of anaerobic respiration in microbial resistance. *Biochem. Biophys. Res. Commun.* **424**(4), 657–662. https://doi.org/10.1016/j.bbrc.2012.06.134 (2012).
137. Gopinath, P., Gogoi, S. K., Chattopadhyay, A. & Ghosh, S. S. Implications of silver nanoparticle induced cell apoptosis for in vitro gene therapy. *Nanotechnology* **19**(7), 075104. https://doi.org/10.1088/0957-4484/19/7/075104 (2008).
138. Lopes, J. et al. Safety of gold nanoparticles: From in vitro to in vivo testing array checklist. *Pharmaceutics* **15**(4), 4. https://doi.org/10.3390/pharmaceutics15041120 (2023).
139. Brennan, S. A. et al. Silver nanoparticles and their orthopaedic applications. *Bone Jt. J.* **97**(5), 582–589. https://doi.org/10.1302/0301-620X.97B5.33336 (2015).
140. Dos Santos, C. A. et al. Silver nanoparticles: Therapeutical uses, toxicity, and safety issues. *J. Pharm. Sci.* **103**(7), 1931–1944. https://doi.org/10.1002/jps.24001 (2014).
141. Noga, M., Milan, J., Frydrych, A. & Jurowski, K. Toxicological aspects, safety assessment, and green toxicology of silver nanoparticles (AgNPs)—critical review: State of the art. *Int. J. Mol. Sci.* **24**, 6. https://doi.org/10.3390/ijms24065133 (2023).
142. Al-Otibi, F. et al. Comparative study of antifungal activity of two preparations of green silver nanoparticles from *Portulaca oleracea* extract. *Saudi J. Biol. Sci.* **29**(4), 2772–2781. https://doi.org/10.1016/j.sjbs.2021.12.056 (2022).

Acknowledgements
The authors express their gratitude to the African Union for their support in this project through the Pan African University Institute for Basic Sciences, Technology, and Innovation (PAUSTI). We extend our gratitude to the chemistry laboratory of Jomo Kenyatta University of Agriculture and Technology for providing facilities for conducting our study. Additionally, we would like to express our appreciation to the Horticulture Students Association for providing the facilities that allowed us to grow our microgreens. We acknowledge PAUSTI Molecular Biology laboratory and M. Patrick KOECH, Lab technician, for allowing us to conduct this research in their facilities. We extend our gratitude to Dennis Mwanza Nzilu for his valuable advice and suggestions.

Author contributions
D.S., J.B., J.W., and S.W. conceived and designed the study. D.S. carried out experiments and collected data, analyzed, interpreted data, and drafted the manuscript. All the authors have made comments on the first versions of the manuscript. All authors have reviewed and edited the manuscript. All authors read and approved the manuscript.

Declarations

Competing interests
The authors declare no competing interests.

Additional information
Supplementary Information The online version contains supplementary material available at https://doi.org/10.1038/s41598-024-80528-6.

Correspondence and requests for materials should be addressed to D.S.

Reprints and permissions information is available at www.nature.com/reprints.

Publisher's note Springer Nature remains neutral with regard to jurisdictional claims in published maps and institutional affiliations.

Open Access This article is licensed under a Creative Commons Attribution-NonCommercial-NoDerivatives 4.0 International License, which permits any non-commercial use, sharing, distribution and reproduction in any medium or format, as long as you give appropriate credit to the original author(s) and the source, provide a link to the Creative Commons licence, and indicate if you modified the licensed material. You do not have permission under this licence to share adapted material derived from this article or parts of it. The images or other third party material in this article are included in the article's Creative Commons licence, unless indicated otherwise in a credit line to the material. If material is not included in the article's Creative Commons licence and your intended use is not permitted by statutory regulation or exceeds the permitted use, you will need to obtain permission directly from the copyright holder. To view a copy of this licence, visit http://creativecommons.org/licenses/by-nc-nd/4.0/.

© The Author(s) 2024